MDPI

Article

Mineral Chemistry and Trace Element Composition of Clinopyroxenes from the Middle Cambrian Ust'-Sema Formation Ankaramites and Diopside Porphyry Basalts and the Related Barangol Complex Intrusions, Gorny Altai, Russia

Nezar Khlif [1], Andrey Vishnevskiy [1,2,*], Andrey Izokh [1,2] and Maria Chervyakovskaya [3]

[1] Sobolev Institute of Geology and Mineralogy, Siberian Branch Russian Academy of Sciences, 630090 Novosibirsk, Russia; nezar.khlif@mail.ru (N.K.); izokh@igm.nsc.ru (A.I.)
[2] Department of Geology and Geophysics, Novosibirsk State University, 630090 Novosibirsk, Russia
[3] Zavaritsky Institute of Geology and Geochemistry, Ural Branch Russian Academy of Sciences, 620016 Yekaterinburg, Russia; masha_vuf_91@mail.ru
* Correspondence: vishnevsky@igm.nsc.ru

Abstract: The origin and geodynamic settings of the Ust'-Sema Formation and the Barangol Complex are some of the most controversial issues in the Early Paleozoic history of the Altai–Sayan Fold Belt. The Ust'-Sema Formation volcanic rocks are enriched in high-Ca clinopyroxene phenocrysts and were classified as ankaramites and diopside porphyry basalts. In this work, we first present LA-ICP-MS analyses of the clinopyroxenes, along with studies of the petrography, mineral composition, and whole-rock chemistry of the Ust'-Sema Formation and related Barangol Complex rocks. An LA-ICP-MS clinopyroxene study showed a slight depletion of light rare-earth elements $(La/Yb)_N = 0.1–1.0$ (on average 0.4); and strong depletion of the high-field-strength elements (Zr, Hf, and Nb) and large-ion lithophile (Rb) elements. An Sr anomaly showed a positive correlation with Mg#. Major- and trace-element composition of the clinopyroxene cores show that these clinopyroxene grains were not captured from the mantle rocks as previously assumed and that the Ust'-Sema Formation and the Barangol Complex rocks were formed from magma with island arc characteristics. The increased titanium and light rare-earth element contents in the phenocryst rims from Biyka volcano suggest an active interaction of the ankaramitic magma with rocks or melts of OIB type.

Keywords: ankaramites; diopside-rich rocks; LA-ICP-MS; clinopyroxene phenocrysts; Ural-Alaskan-type intrusions

1. Introduction

The genesis of Early Paleozoic volcanic and intrusive complexes in Gorny Altai (in the western part of the Altai–Sayan Fold Belt) is a controversial issue. Previous researchers attributed them to either the magmatism of back-arc basins and island arcs or continental margin rifting, or a mid-ocean ridge subduction and suprasubduction setting combination [1–10]. These magmatic associations include Middle Cambrian volcanic rocks of the Ust'-Sema Formation and intrusions of the Barangol Complex.

The Ust'-Sema Formation volcanics are enriched in clinopyroxene phenocrysts and are classified into two groups: ankaramites and diopside porphyry basalts (Di-basalts) [10]. These rocks are spatially associated with ultramafic–mafic intrusions of the Barangol Complex considered to be comagmatic to volcanic rocks of the Ust'-Sema Formation [4–6].

Previous investigations of the Ust'-Sema Formation were focused on the rocks' major- and trace-element compositions, aimed at reconstructing the geodynamic settings [4,7,8]. However, the origin of magmatic protoliths of the Barangol Complex intrusions is still poorly understood.

Clinopyroxene is one of the main rock-forming minerals for the rocks of the Ust'-Sema Formation and the Barangol Complex. It is better preserved in contrast to plagioclase, which, in most cases, is completely altered. Since the composition of clinopyroxene mainly depends on the primary magma characteristics and the crystallization environment, therefore, it is strongly affected by geodynamic settings [11–18]. Major- and trace-element compositions of clinopyroxene in igneous rocks have widely been used to determine these geodynamic settings and the nature of the parental magma [17].

In this paper, we present a study on the petrography, mineral composition, and chemistry of the rocks, along with data from the major- and trace-element composition of clinopyroxene. Our purpose was to use the major- and trace-element compositions of clinopyroxene to determine the specific features and nature of the Ust'-Sema Formation and the Barangol Complex. This will also allow for an evaluation of the relationship between the Ust'-Sema Formation volcanics and the Barangol Complex intrusions.

2. Geological Setting

Gorny Altai is located in the west of the Altai–Sayan folded area, which is in the northern part of the Central Asian folded belt [19]. This area extends to the territories of Russia, Kazakhstan, northern China, and Mongolia. Gorny Altai includes the Kurai and Katun' accretionary complexes (wedges). The Katun' accretionary complex was formed as a result of Late Neoproterozoic–Cambrian subduction of the Paleo-Asian oceanic crust and accretion of oceanic islands to the Kuznetsk–Altai island arc [3,5].

The study area of the Katun' accretionary complex (northern Gorny Altai) consists of tectonic blocks and volcanogenic–sedimentary units that are interpreted as various lithological facies of the Early Cambrian Katun' seamount and underlying Late Neoproterozoic–Early Cambrian rocks of oceanic floor and ophiolite association [5,8].

The Ust'-Sema Formation overlies the Katun' accretionary complex. This formation is widespread along the banks of the Katun' River and in the basins of its left and right tributaries—the Sema and Biyka rivers (Figure 1). The Ust'-Sema Formation volcanics are localized primarily in two central-type volcanic edifices: Ust'-Sema in the northwest and Biyka in the southeast of the Katun' zone (Figure 1). The Anos-Emurla's linear structure extends over 90 km between the two central-type volcanic edifices. In addition, Ust'-Sema volcanic rocks are found in areas near Kamlak village (12 km west of Ust'-Sema village along the Sema River) and Kuyus village (20 km south of the Biyka volcano) (Figure 1). The Ust'-Sema Formation includes flows of pyroxene porphyry and pyroxene–plagioclase porphyry basalts, agglomerates, pyroclastic breccias, and tuffs.

The Ust'-Sema Formation rocks rest upon the Neoproterozoic–lower Cambrian sediments of the Cheposh and Manzherok Formations (Figure 1) and are overlain, with an angular unconformity, by the Elanda Formation, containing trilobites typical of the upper part of the middle Cambrian [6,20]. The Ust'-Sema Formation are associated with the dikes and subvolcanic bodies of the Barangol Complex [4]. The volume and composition of the Barangol intrusions is debatable and interpreted differently by researchers. Previously, all the Early Paleozoic ultramafic–mafic bodies, which intrude the Neoproterozoic–Cambrian Katun' Complex assemblages, were "combined" into the Barangol Complex [6]. Later, three types of intrusions were identified from the Barangol Complex: the Apshiyakhta intrusion of dunite–wehrlite–clinopyroxenite; the Elanda intrusion of syenite–monzodiorite–monzogabbro; and the Barangol intrusion of diorite–pyroxenite–gabbro [21]. The age of the Barangol Complex was determined as Middle Cambrian (510.4 ± 2.4 Ma) by the U–Pb method using zircon from leucogabbro [22].

The Barangol intrusion is located in the area of the Barangol River and is spatially confined to the Ust'-Sema volcanic edifice (Figure 1d). It consists of pyroxenites, gabbro with quenching zones of gabbro–dolerite composition, diorites, and quartz diorites. Elanda and Apshiyakhta intrusions are located near the Biyka volcanic edifice (Figure 1c). The Elanda intrusion (area 0.1 km^2) is composed mainly of medium-grained gabbro, monzogabbro, monzodiorite, and minor gabbro–dolerite. The Apshiyakhta intrusion is located on

the left side of the Apshiyakhta River near its confluence to the Katun' River and consists of wehrlite, clinopyroxenite, and gabbro. A number of gabbroic bodies intruding the volcanic rocks of the Biyka volcanic edifice in the Choburak River area have been observed (Figure 1c). They are mainly composed of gabbro and melagabbro. In this research, the gabbroic bodies of the Choburak area were also considered as Barangol Complex intrusions.

In this paper, the authors studied Ust'-Sema Formation volcanic rocks from the Ust'-Sema, Anos-Emurla, and Biyka volcanic edifices as well as from the Kamlak unit. One sample from the Kuyus was studied and added to the Biyka set. Barangol Complex rocks were also studied from the Apshiyakhta, Elanda, and Barangol intrusions as well as from the Choburak area.
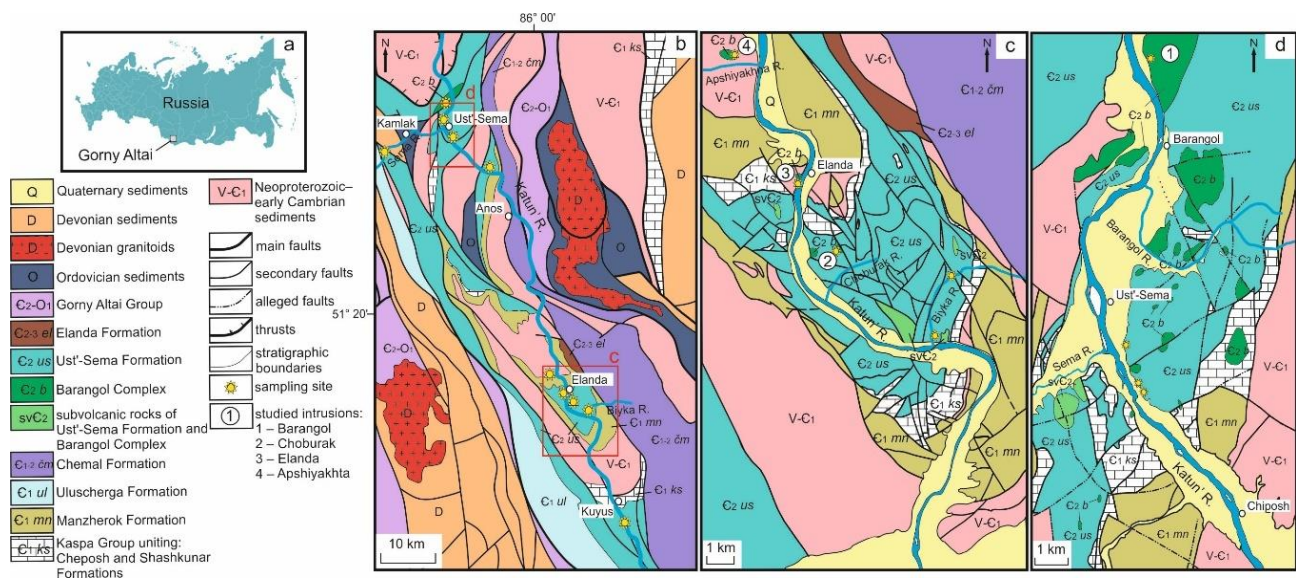

Figure 1. (**a**) Location map of Gorny Altai, Russia; (**b**) simplified geological map of northern Gorny Altai [20]; (**c**) geological map of the Biyka volcanic edifice of the Ust'-Sema Formation [6]; (**d**) geological map of the Ust'-Sema volcanic edifice of the Ust'-Sema Formation [6].

3. Analytical Methods

For this study, seven samples of volcanic rocks from the Ust'-Sema Formation were taken from the Biyka, Ust'-Sema, and Anos-Emurla volcanic edifices and the Kamlak unit. Six samples were taken from the intrusions of Elanda, Barangol, and Choburak of the Barangol Complex.

Thin and polished sections were prepared from the samples for petrographic study. Sampled clinopyroxene crystals were mounted in epoxy-resin blocks. The blocks and the polished sections were examined using an Oxford X-Max 80 energy-dispersive spectrometer (EDS) with a TESCAN MIRA 3 scanning electron microscope (SEM) at the Analytical Center for Multi-Elemental and Isotope Research SB RAS at the Sobolev Institute of Geology and Mineralogy (IGM SB RAS), Novosibirsk.

Operation conditions: spectrum acquisition time, 20–30 s; voltage, 20 kV; current, 10 nA. The error in measurement was 0.4–3.0% for major components and 4–7% for trace elements. The detection limit of the components was 0.01–0.02 wt.% (3σ criterion) [23]. The spectral data were processed using the INCA Energy 5.05 software (Oxford Instruments, Oxfordshire, UK).

Trace-element analyses of clinopyroxene were carried out using the laser ablation with an inductively coupled plasma mass spectrometry (LA ICP-MS) technique. For the analysis, 26 grains were selected: 17 grains from the Ust'-Sema Formation and 9 grains from the intrusions of the Barangol Complex. Examinations were conducted with a NexION 300S (PerkinElmer, Waltham, MA, USA) ICP-MS, equipped with an NWR213 (ESI) laser-ablation system in "Geoanalitik" shared research facilities at the IGG UB RAS (Zavaritsky Institute

of Geology and Geochemistry, Yekaterinburg). The laser spot diameter was 50 μm, and the operating time 50 s. A study of the clinopyroxene crystals' zoning was also carried out using LA-ICP-MS profiles in two ways: either along the entire crystal or starting from the core to the outer zone. The data processing was performed using the Glitter 4.4 software (GEMOC, Sydney, Australia). The SiO_2 concentrations obtained via EDS were used as the internal standard, NIST SRM 612, and reference glass was used as the external standard measured after every 10 points. The rare-earth element detection limit was 0.01 ppm.

The bulk composition of the rocks was analyzed by X-ray fluorescence analysis (XRF) on a Thermo Scientific ARL-9900 XP spectrometer at the Analytical Center for Multi-Elemental and Isotope Research (IGM SB RAS), Novosibirsk. The sample powder was fused at a ratio of 1:9 with a mixture of lithium tetraborate and lithium metaborate to prepare glass beads. The detection limit for major elements was 30 ppm.

4. Results

4.1. Petrography

4.1.1. The Ust'-Sema Formation Volcanic Rocks

The volcanic rocks of the Ust'-Sema Formation (Figure 2) were characterized by a massive structure and a porphyritic texture. These rocks were mostly gray to dark gray with a green tint, and sometimes with a red tint that is typical of Kamlak unit rocks.

The mineral composition, petrography, and chemistry of the volcanic rocks from the Biyka volcanic edifice were studied in detail in previous work [10]. The rocks were subdivided into two main groups: ankaramites and diopside porphyry basalts. Criteria for the identification of ankaramites included an abundance of clinopyroxene phenocrysts and a high $CaO/Al_2O_3 > 1$ ratio [10,24]. In the present study, according to these criteria, ankaramites were also identified among the volcanic rocks of the Ust'-Sema Formation in other areas (Table 1).

The ankaramites of the Ust'-Sema Formation were characterized by abundant phenocrysts of clinopyroxene (25–50 vol.%) enclosed in the clinopyroxene–plagioclase microlitic groundmass (Figure 2a,c,e). In contrast, phenocrysts of plagioclase were usually dominant in the diopside porphyry basalts (Figure 2b,d). Sometimes there were amphibole, and what are believed to be completely altered olivine phenocrysts (very rare), and grains of Cr-spinel. Cr-spinel occurs as small inclusions within clinopyroxene phenocrysts in both ankaramites and diopside porphyry basalts. The groundmass consists of clinopyroxene, plagioclase, K-feldspar, apatite, quartz, muscovite, and titanite. Calcite is a common secondary mineral, especially in the Kamlak unit, and also exists in several samples from the Biyka and Ust'-Sema volcanic edifices. This can significantly affect the bulk-rock composition and leads to an increase in the loss-on-ignition (LOI) value and CaO concentration (Figure 2f; Table 1).

4.1.2. The Intrusions of the Barangol Complex

The gabbro of the Barangol intrusion was strongly altered. The sample had a medium and fine-grained texture and was characterized by a typical gabbro (allotriomorphic) texture, consisting of hypidiomorphic clinopyroxene and altered plagioclase crystals (Figure 3b).

The rocks from the Elanda intrusion were represented by three types: monzodiorite, gabbro, and melagabbro (Figure 3a–c). The monzodiorite had a hypidiomorphic texture with a highly idiomorphic altered plagioclase and clinopyroxene crystals relative to K-feldspar (Figure 3a). The gabbro was characterized by a typical gabbro (allotriomorphic) texture, consisting of clinopyroxene and altered plagioclase crystals (Figure 3b). Melagabbro was characterized by hypidiomorphic texture and consisted of euhedral clinopyroxene crystals, xenomorphic grains of altered plagioclase, and rarely amphibole (Figure 3c).
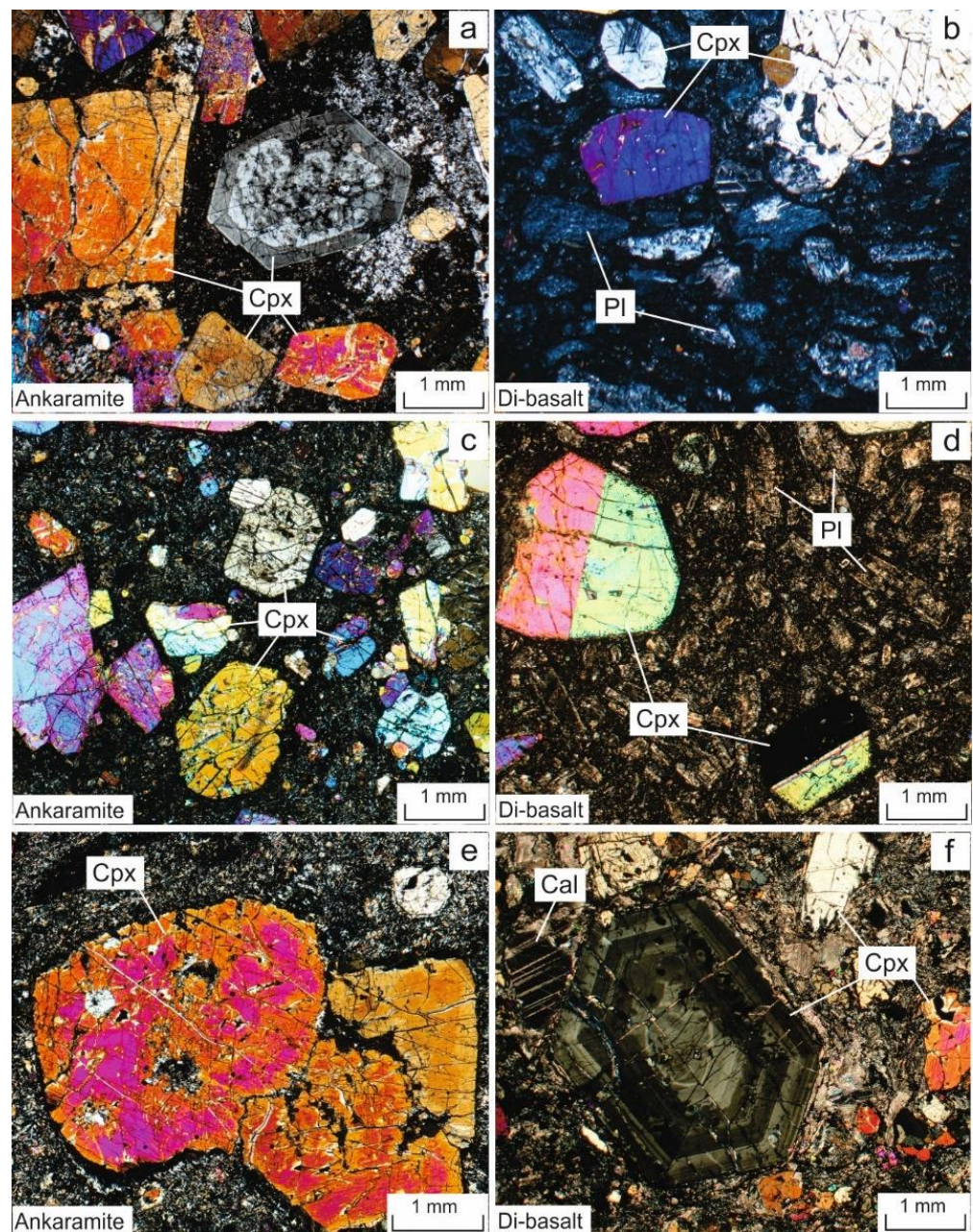
Figure 2. Microphotographs of thin sections of the Ust'-Sema Formation volcanic rocks, Gorny Altai, (cross-polarized light): (**a**,**b**) Biyka volcanic edifice; (**c**,**d**) Ust'-Sema volcanic edifice; (**e**) Anos-Emurla volcanic edifice; (**f**) Kamlak unit. Cal—calcite; Cpx—clinopyroxene; Pl—plagioclase.

The rocks of the Apshiyakhta intrusion, in most cases, were also strongly altered. In the preserved samples, they were represented by phlogopite–olivine clinopyroxenite (Phl-Ol clinopyroxenite). The rocks had a hypidiomorphic texture with highly idiomorphic olivine crystals (Figure 3f). Sometimes a poikilitic texture was observed where clinopyroxene oikocrysts included small olivine grains.

The Choburak intrusions were represented by gabbro with a porphyritic texture generally consisting of large subhedral crystals of clinopyroxene and small grains of altered plagioclase (Figure 3e).

Table 1. Major element composition of the rocks from the Ust'-Sema Formation and the Barangol Complex, Gorny Altai.

Location	Rock Type	Sample	SiO_2	TiO_2	Al_2O_3	Fe_2O_3 *	MnO	MgO	CaO	Na_2O	K_2O	P_2O_5	Cr_2O_3	LOI	Total	CaO/Al_2O_3
						Ust'-Sema Formation										
Biyka	Ankaramite	BIY-05-17 **[(1)]	48.61	1.10	10.45	10.43	0.16	10.97	12.09	2.30	0.49	0.12	0.09	2.40	99.33	1.2
		BIY-04-17 **	44.78	1.05	13.41	10.95	0.20	8.27	14.48	0.77	1.07	0.37	0.03	3.37	99.88	1.1
	Di-basalt	BIY-02-18	47.98	1.11	13.74	11.25	0.18	7.84	11.56	2.28	0.31	0.16	0.04	3.22	99.87	0.8
		BIY-01-02-17 **	46.37	1.00	15.80	9.74	0.16	7.03	11.86	1.78	1.63	0.12	0.05	3.68	99.53	0.8
		BIY-01-03-17 **	44.02	0.84	12.41	9.46	0.22	7.25	15.69	2.26	0.60	0.10	0.04	6.35	99.55	1.3
		BIY-01-04-17 **	43.66	0.82	13.26	8.90	0.22	5.42	16.84	2.20	0.13	0.17	0.03	7.47	99.39	1.3
Ust'-Sema	Ankaramite	KAT-06-18	47.87	0.44	10.02	10.25	0.17	13.01	12.66	0.61	0.10	0.12	0.13	4.70	100.23	1.3
	Di-basalt	KAT-5-18	47.94	0.47	9.91	9.83	0.16	10.80	13.37	1.01	0.14	0.12	0.14	5.85	99.95	1.3
		BAR-07-18	45.91	0.88	16.02	11.45	0.18	7.74	11.82	2.16	0.68	0.19	0.03	2.21	99.45	0.7
		BIY-07-17	49.07	0.69	16.67	9.87	0.17	6.35	9.79	2.79	1.09	0.20	0.02	2.64	99.47	0.6
Anos-Emurla	Ankaramite	ANO-01-18	49.19	0.34	7.43	11.53	0.20	14.34	12.23	0.87	0.58	0.20	0.15	2.71	99.89	1.6
Kamlak	Di-basalt	KAM-01-18	40.06	0.60	9.21	12.92	0.14	8.61	16.44	0.08	2.19	0.04	0.11	9.34	99.96	1.8
						Barangol Complex										
Elanda	Monzodiorite	ELN-01-17	49.60	0.51	21.13	8.40	0.15	2.68	7.23	3.45	3.41	0.24	<0.01	2.61	99.57	0.3
	Gabbro	ELN-02-17	45.47	0.49	14.45	7.24	0.11	8.53	17.84	0.89	1.35	0.05	<0.01	2.82	99.34	1.2
	Melagabbro	ELN-03-17	47.52	0.44	9.46	9.10	0.16	12.42	16.44	1.32	0.84	0.09	0.06	2.10	100.04	1.7
Apshiyakhta	Phl-Ol clinopyroxenite	APSH-05-17	47.98	0.57	10.22	9.61	0.18	16.09	9.06	1.57	0.96	0.12	0.20	2.39	99.09	0.9
Barangol	Gabbro	BAR-02-15	44.75	0.68	13.90	12.04	0.21	10.60	11.86	1.14	1.07	0.22	0.07	2.64	99.33	0.9
Choburak	Gabbro	KAT-02-18	46.51	0.58	10.45	10.72	0.17	12.70	13.24	1.06	1.17	0.14	0.13	3.20	100.20	1.3

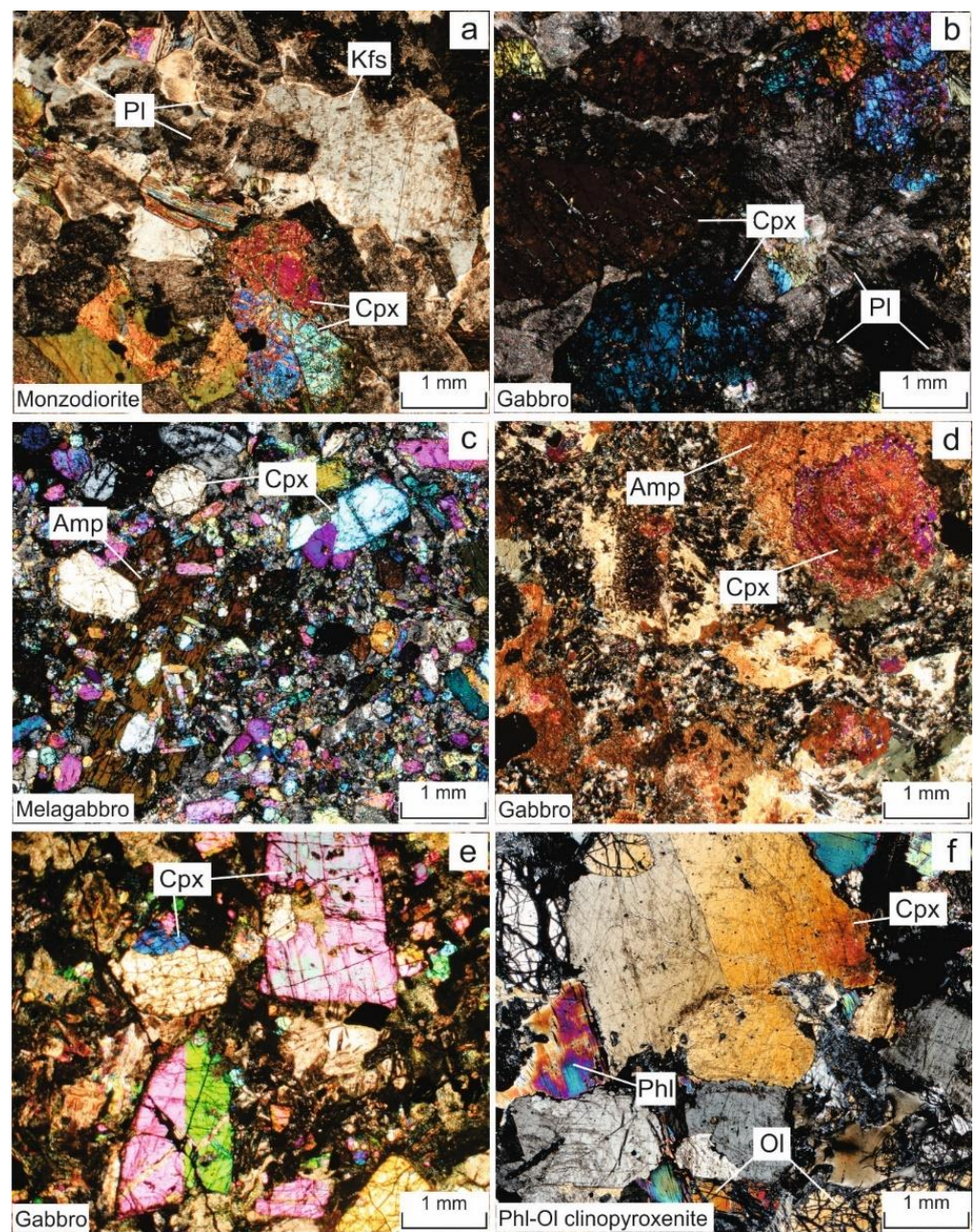* Total iron as Fe_2O_3; ** samples were considered in a previous work [10]. [(1)] Sample from the Kuyus site.

Figure 3. Microphotographs of thin sections of the rocks from different intrusions of the Barangol Complex, Gorny Altai (cross-polarized light): (**a**–**c**) Elanda intrusion; (**d**) Barangol intrusion; (**e**) Choburak intrusions; (**f**) Apshiyakhta intrusion. Amp—amphibole; Cpx—clinopyroxene; Kfs—K-feldspar; Ol—olivine; Phl—phlogopite; Pl—plagioclase.

4.2. Whole Rock Chemistry

On the TAS diagram, the volcanic rocks of the Ust'-Sema Formation were mostly in the field of basalts and rarely in the field of picrobasalts (Figure 4a). Depending on the CaO/Al_2O_3 ratio (Figure 4b), these rocks could be divided into two groups: ankaramites with a CaO/Al_2O_3 ratio > 1 and diopside porphyry basalts with a CaO/Al_2O_3 ratio < 1 (Figure 4b).

Despite this, some samples from diopside porphyry basalts had a ratio of $CaO/Al_2O_3 > 1$, meaning that these rocks cannot be classified as ankaramites (Figure 4b) because they have a high loss on ignition (LOI = 5.85–9.34 wt.%), which is associated with the presence of newly formed calcite in the groundmass (Figures 2f and 4b).
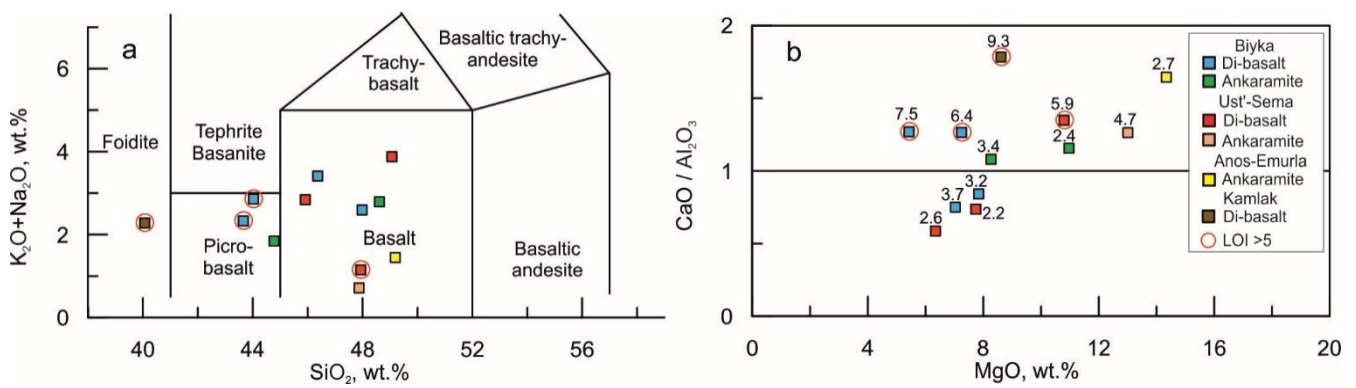
Figure 4. (**a**) TAS diagram [25] and (**b**) variations in MgO vs. CaO/Al_2O_3 for the volcanic rocks of the Ust'-Sema Formation, Gorny Altai. The values indicate the loss on ignition (LOI).

The ankaramites were characterized by high contents of MgO (8.27–14.34 wt.%), CaO (12.09–14.48 wt.%), and high CaO/Al_2O_3 ratio (1.1–1.6), while Al_2O_3 ranged between 7.43 and 13.41 wt.% (Figure 5; Table 1). The diopside porphyry basalts had lower contents of CaO (9.79–11.86 wt.%), MgO (6.35–7.84 wt.%), low CaO/Al_2O_3 ratio (0.6–0.8), and higher contents of Al_2O_3 (13.74–16.67 wt.%) (Figures 4 and 5; Table 1). Meanwhile, some samples of the diopside porphyry basalts with a high LOI (>5 wt.%) had high contents of CaO (13.37–16.84 wt.%) and Cr_2O_3 (on average 0.08 wt.%) (Figure 5).
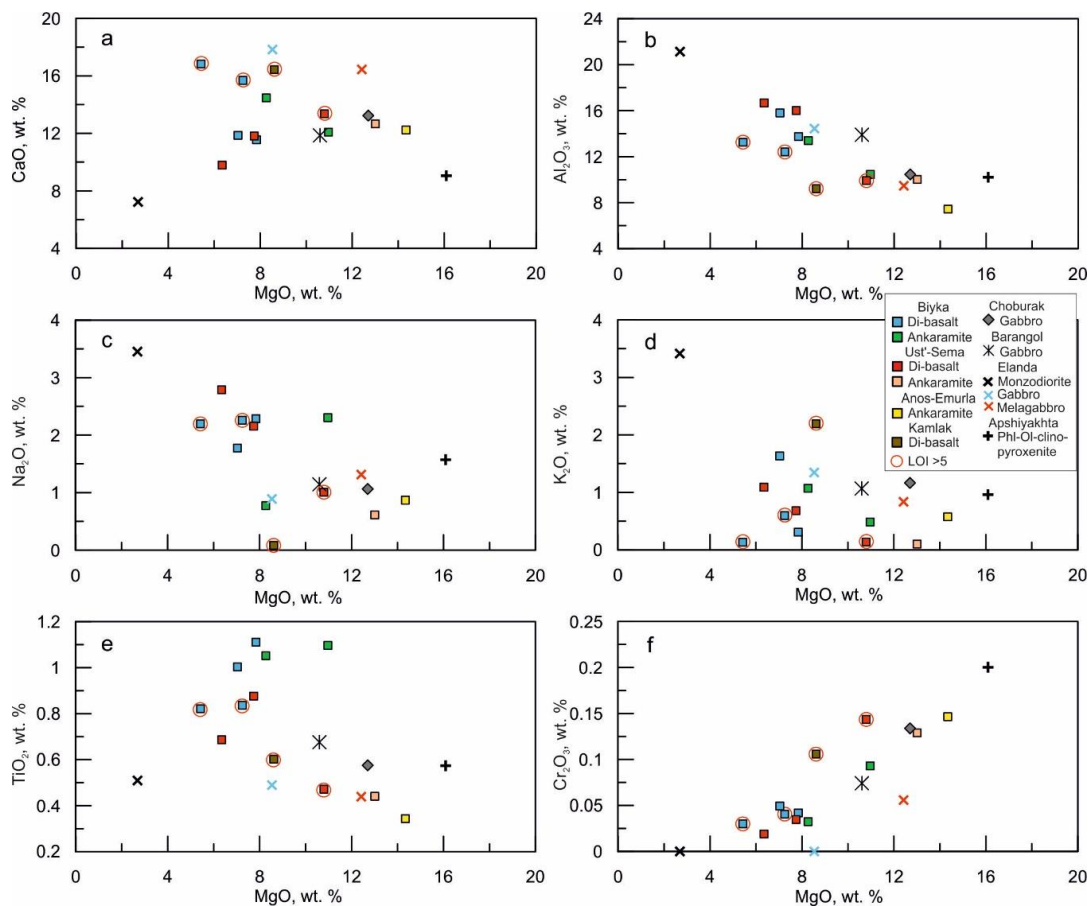

Figure 5. Variations in the MgO content (wt.%) with respect to the contents of other major components for the Ust'-Sema Formation and the Barangol Complex rocks, Gorny Altai. (**a**) MgO vs. CaO; (**b**) MgO vs. Al_2O_3; (**c**) MgO vs. Na_2O; (**d**) MgO vs. K_2O; (**e**) MgO vs. TiO_2; (**f**) MgO vs. Cr_2O_3.

The rocks of the Biyka volcanic edifice had a higher content of TiO_2 (0.82–1.11 wt.%) compared with 0.34–0.88 for the rocks from other areas (Figure 5e). Ankaramite from the Anos-Emurla had a lower content of Al_2O_3 (7.43 wt.%) and a higher content of MgO (14.34 wt.%) compared with Al_2O_3 (9.21–16.67 wt.%) and MgO (5.42–13.01 wt.%) from other areas (Figure 5).

The Ust'-Sema volcanic rocks showed negative correlations of MgO content with Al_2O_3, TiO_2, Na_2O, and K_2O contents and positive correlations with Cr_2O_3 content (Figure 5). Variations in MgO with CaO content did not show correlation (Figure 5a).

Olivine clinopyroxenite from the Apshiyakhta intrusion had the highest MgO and Cr_2O_3 contents (16.09 wt.% and 0.20 wt.%, respectively) among the rocks of the Barangol Complex and Ust'-Sema Formation samples (Figure 5; Table 1). It was characterized by high contents of Al_2O_3 (10.22 wt.%), Na_2O (1.57 wt.%), and Fe_2O_3 (9.61 wt.%) and moderate TiO_2 (0.57 wt.%), CaO (9.06 wt.%), and K_2O (0.96 wt.%) (Figure 5; Table 1).

For the rocks of the Elanda intrusion, MgO content (wt.%) decreased from 12.42 in melagabbro to 8.53 in gabbro and 2.68 in monzodiorite (Figure 5; Table 1). With decreasing MgO content, the contents of Al_2O_3 (9.46–21.13 wt.%), K_2O (0.84–3.41 wt.%), and Na_2O (1.32–3.45 wt.%) increased (Figure 5; Table 1). These rocks were generally characterized by moderate contents of TiO_2 (0.44–0.51 wt.%), Fe_2O_3 (7.24–9.10 wt.%), and Cr_2O_3 (up to 0.06 wt.%) (Figure 5; Table 1). The melagabbro and gabbro from the Elanda intrusion had the highest contents of CaO (16.44 and 17.84 wt.%, respectively) among the Barangol Complex.

The gabbro of the Barangol intrusion was characterized by high contents of MgO (10.6 wt.%), Al_2O_3 (13.9 wt.%), Fe_2O_3 (12.04 wt.%), and TiO_2 (0.68 wt.%); moderate contents of Na_2O (1.14 wt.%), K_2O (1.07 wt.%), and Cr_2O_3 (0.07 wt.%) (Figure 5; Table 1).

The composition of the Choburak gabbro was similar to the Elanda intrusion melagabbro, especially in the MgO, Na_2O, K_2O, and Al_2O_3 contents. However, it contained relatively higher contents of Fe_2O_3, TiO_2, and Cr_2O_3 (Figure 5; Table 1).

4.3. Mineral Chemistry

4.3.1. Clinopyroxene

Major- and trace-element analysis of clinopyroxenes from the rocks of the Ust'-Sema Formation and the Barangol Complex are shown in Table 2, and the whole data set is available in the Table S1.

Clinopyroxene is the main rock-forming mineral for the volcanic rocks of the Ust'-Sema Formation. It occurs as large phenocrysts (2–20 mm, usually 3–9 mm in diameter), microphenocrysts (0.5–1 mm), and microlites in the groundmass (Figures 2 and 6a,b,d,e). Most phenocrysts clearly show zoning in both transmitted light and the BSE images (Figures 2 and 6a,b,d,e). The zoning was mainly normal, less often reverse, and oscillatory (Figures 2 and 6a,b,d,e).

The clinopyroxene phenocrysts cores were mainly composed of diopside $En_{43-50}Wo_{45-48}Fs_{4-11}$ (Figure 7a; Table 2; Supplementary Materials data). They were characterized by high Mg# 92.6–80.0, a wide range of Cr_2O_3 content (0.13–1.11 wt.%; average 0.57 wt.%), a high CaO content (22.12–24.32 wt.%), and low contents of TiO_2 (up to 0.5 wt.%), Al_2O_3 (0.62–4.25 wt.%), and Na_2O (up to 0.36 wt.%) (Figure 7; Table 2; Supplementary Materials).

In contrast, the rims of phenocrysts had a low Mg# 84.4–67.1 with a relatively low Cr_2O_3 content (0.67 wt.%; average 0.30 wt.%) and high contents of Al_2O_3 (up to 8.75 wt.%), TiO_2 (up to 1.78 wt.%), and Na_2O (up to 0.55 wt.%) (Figure 7; Table 2; Supplementary Materials). They were composed of diopside and augite $En_{43-50}Wo_{45-48}Fs_{4-11}$ (Figure 7a; Table 2; Supplementary Materials).

Clinopyroxene phenocrysts from the Biyka volcanic edifice had the highest contents of TiO_2 (up to 1.78 wt.%), Al_2O_3 (up to 8.75 wt.%), and Na_2O (up to 0.55 wt.%) compared with other areas that were characterized by low contents of TiO_2 (up to 0.77 wt.%), Al_2O_3 (up to 4.25 wt.%), and Na_2O (up to 0.43 wt.%) (Figure 7; Table 2; Supplementary Materials).

Table 2. Major (by SEM-EDS) and trace (by LA-ICP-MS) element compositions of the clinopyroxene from the Ust'-Sema Formation and the Barangol Complex rocks, Gorny Altai.

Location	Biyka				Ust'-Sema				Anos-Emurla	
Sample	BIY-01-02-17		BIY-04-17		KAT-05-18		KAT-06-18		ANO-01-18	
Note	C	R	C	R	C	R	C	R	C	R
SiO$_2$ (wt.%)	50.75	48.58	53.78	45.93	53.48	52.46	54.10	50.96	51.99	51.45
TiO$_2$	0.43	1.02	<dl	1.63	<dl	<dl	<dl	0.42	<dl	0.23
Al$_2$O$_3$	3.16	4.67	0.94	7.46	1.28	2.95	0.89	3.87	1.66	2.87
Cr$_2$O$_3$	0.64	<dl	0.72	<dl	0.64	0.28	0.66	0.15	1.08	0.67
FeO	4.73	9.12	3.32	9.35	3.99	6.36	3.13	7.77	4.43	6.34
MnO	<dl	0.26	<dl	0.25	<dl	0.15	<dl	0.23	<dl	0.26
MgO	16.02	13.65	17.76	11.49	17.36	16.02	18.16	15.14	16.17	16.30
CaO	23.02	21.25	23.02	23.06	23.04	22.28	22.96	21.83	23.45	21.16
Na$_2$O	<dl	0.30	0.12	<dl	0.13	0.22	0.18	0.24	<dl	0.32
Total	98.75	98.85	99.66	99.18	99.94	100.70	100.07	100.61	98.78	99.61
Mg#	85.7	72.8	90.6	68.7	88.6	81.8	91.2	77.7	86.7	82.0
Fs	7.6	15.0	5.1	15.7	6.2	10.0	4.8	12.4	7.0	10.2
Wo	47.0	44.9	45.8	49.8	45.8	45.0	45.3	44.6	47.5	43.4
En	45.5	40.1	49.1	34.5	48.0	45.0	49.8	43.0	45.5	46.5
V (ppm)	325.28	666.35	73.98	785.92	111.57	283.34	67.87	401.37	132.02	190.72
Ni	102.56	35.92	161.53	78.23	141.09	107.28	181.67	110.55	127.31	117.22
Rb	0.0580	0.0800	<dl	0.3440	<dl	0.0090	0.2540	0.0098	1.1200	<dl
Sr	19.01	24.96	29.25	162.22	33.81	34.5	43.96	100.77	49.96	57.66
Y	5.86	16.86	2.59	21.83	2.26	7.21	2.17	11.27	3.95	7.59
Zr	5.16	15.67	0.80	57.27	0.90	4.57	<dl	7.20	1.75	4.28
Nb	0.042	0.024	<0,00	1.030	0.035	<dl	0.022	<dl	<dl	<dl
Cs	0.0159	0.0430	0.0260	0.1720	0.0068	0.0160	0.1750	0.1150	0.0570	0.0170
Ba	1.70	1.28	<dl	53.22	0.12	<dl	0.82	0.63	13.44	0.28
La	0.211	0.740	0.155	6.660	0.080	0.366	0.086	0.348	0.071	0.500
Ce	1.110	3.450	0.474	22.620	0.496	1.330	0.450	2.000	0.640	2.090
Pr	0.320	0.880	0.092	4.110	0.119	0.365	0.087	0.433	0.241	0.441
Nd	1.78	6.30	0.81	21.08	0.73	2.22	0.62	3.28	2.22	2.37
Sm	1.09	2.33	0.50	5.49	0.57	0.84	<dl	1.07	0.54	1.19
Eu	0.353	0.940	0.169	1.830	0.102	0.392	0.065	0.484	0.205	0.600
Gd	1.05	4.10	0.66	5.23	0.40	1.19	0.22	2.67	1.00	1.84
Tb	0.231	0.700	0.045	0.830	0.065	0.179	0.048	0.273	0.089	0.117
Dy	1.49	3.48	0.45	4.97	0.39	1.40	0.21	2.11	0.57	1.48
Ho	0.310	0.840	0.189	0.780	0.096	0.340	0.114	0.562	0.124	0.560
Er	0.87	1.99	0.11	2.05	0.21	0.48	0.49	0.95	0.42	1.19
Tm	0.090	0.293	0.051	0.310	0.015	0.064	<dl	0.085	0.070	0.203
Yb	0.590	1.430	0.077	2.620	0.270	0.600	0.680	0.680	0.300	0.620
Lu	0.048	0.289	0.013	0.309	0.048	0.047	<dl	0.134	0.025	0.063
Hf	0.312	1.050	0.063	2.210	0.041	0.370	<dl	0.245	0.129	0.055
Ta	0.0074	<dl	<dl	0.1590	<dl	<dl	<dl	<dl	<dl	<dl
Th	<dl	<dl	<dl	0.155	0.0089	0.022	<dl	<dl	<dl	<dl
U	<dl	0.0071	<dl	0.043	<dl	<dl	0.021	<dl	<dl	<dl
(La/Yb)$_N$	0.2	0.3	1.4	1.7	0.2	0.4	0.1	0.3	0.2	0.5
Eu/Eu*	1.0	0.9	0.9	1.0	0.7	1.2	<dl	0.9	0.9	1.2
Sample	KAM-01-18		ELN-01-17	ELN-02-17	ELN-03-17	APSH-05-17	BAR-02-15	KAT-02-18	
Note	C	R	C	C	C	C	C	C	R
SiO$_2$ (wt.%)	48.35	50.00	51.00	48.44	52.41	53.48	51.15	50.87	50.04
TiO$_2$	0.60	0.33	0.23	0.73	0.23	0.15	0.65	0.27	0.95
Al$_2$O$_3$	5.46	3.40	1.95	4.99	3.02	2.23	3.02	2.74	3.02
Cr$_2$O$_3$	<dl	<dl	<dl	<dl	0.19	0.94	0.29	0.32	<dl
FeO	8.47	7.71	14.70	8.75	5.67	3.65	8.88	5.96	11.48
MnO	0.18	<dl	0.50	<dl	<dl	<dl	0.28	<dl	0.34
MgO	13.32	14.21	10.51	12.82	15.55	17.35	14.10	15.12	12.30
CaO	23.53	23.63	21.20	21.95	24.25	22.96	21.39	23.56	21.98
Na$_2$O	0.30	0.19	0.46	0.49	<dl	0.18	0.47	<dl	0.38
Total	100.20	99.47	100.56	98.16	101.34	100.93	100.39	98.84	100.49
Mg#	73.7	76.7	56.0	72.3	83.0	89.5	73.9	81.9	65.7
Fs	13.6	12.2	24.3	14.6	8.8	5.7	14.5	9.5	18.63
Wo	48.4	47.8	44.8	47.1	48.2	46.0	44.6	47.8	45.75
En	38.0	40.0	30.9	38.2	43.0	48.3	40.9	42.7	35.62

Table 2. *Cont.*

Location	Biyka				Ust'-Sema			Anos-Emurla	
V (ppm)	239.65	228.76	233.42	368.37	253.70	177.37	223.13	181.72	408.83
Ni	129.83	118.50	15.61	82.73	102.83	240.08	119.70	118.86	88.39
Rb	2.32	0.22	<dl	3.1	<dl	<dl	<dl	<dl	0.24
Sr	146.42	148.13	44.64	55.35	46.42	46.89	46.98	43.06	53.86
Y	21.66	11.90	48.29	14.69	5.94	3.60	18.71	6.87	17.22
Zr	24.69	20.63	48.42	36.36	5.56	1.98	18.13	4.32	15.35
Nb	<dl	0.33	0.28	0.30	<dl	0.038	<dl	<dl	0.08
Cs	1.34	<dl	2.47	0.089	<dl	0.018	<dl	<dl	0.02
Ba	3.94	1.54	2.11	7.05	0.09	2.49	1.62	0.70	5.37
La	1.43	1.09	3.93	1.41	0.24	0.24	1.39	0.20	0.90
Ce	3.84	3.25	13.36	4.39	1.22	0.75	4.40	0.80	2.40
Pr	0.780	0.810	2.300	0.750	0.336	0.219	1.470	0.199	0.680
Nd	5.45	4.32	14.68	4.77	1.57	1.28	6.16	1.56	5.01
Sm	3.57	1.65	5.63	1.57	0.68	0.41	1.45	0.79	2.39
Eu	0.750	0.600	1.140	0.860	0.233	0.103	0.980	0.217	0.600
Gd	1.73	2.41	8.51	2.58	1.68	0.49	2.77	1.37	2.60
Tb	0.191	0.320	1.370	0.436	0.120	0.108	0.510	0.186	0.492
Dy	3.99	1.97	12.05	2.54	1.07	0.68	2.96	1.43	3.66
Ho	0.730	0.740	1.960	0.670	0.333	0.167	0.860	0.281	0.668
Er	1.11	1.65	7.04	1.77	1.40	0.61	2.15	1.06	1.52
Tm	0.350	0.153	1.010	0.270	0.061	0.022	0.239	0.155	0.203
Yb	1.53	0.94	4.95	0.95	0.75	0.40	2.00	0.61	1.94
Lu	0.350	0.124	1.050	0.305	0.062	0.068	0.292	0.167	0.264
Hf	1.440	0.730	1.680	2.080	0.420	0.233	0.420	0.440	0.730
Ta	<dl	<dl	0.086	0.078	<dl	<dl	0.031	<dl	0.019
Th	0.0480	<dl	<dl	0.1190	<dl	<dl	0.0250	0.0086	0.0160
U	0.081	<dl	0.092	0.120	<dl	<dl	<dl	<dl	<dl
$(La/Yb)_N$	0.6	0.8	0.5	1.0	0.2	0.4	0.5	0.2	0.31
Eu/Eu*	0.9	0.9	0.5	1.3	0.7	0.7	1.5	0.6	0.74

(<dl)—below detection limit; $(La/Yb)_N$—chondrite-normalized [26]. Eu* = $\sqrt{(Sm_N \times Gd_N)}$; Mg# = 100 Mg/(Mg + Fe).

In the case of reverse zoning, for example, in the diopside porphyry basalts of the Kamlak unit, the cores of the clinopyroxene phenocrysts had a low Mg# 75.4–72.2 with high contents of Al_2O_3 (3.85–5.46 wt.%), TiO_2 (0.60–0.75 wt.%), and Na_2O (0.20–0.30 wt.%) (Figure 7; Table 2). However, the rims of phenocrysts had a relatively high Mg# 76.7–76.2 with low contents of Al_2O_3 (3.16–3.40 wt.%), TiO_2 (0.33–0.48 wt.%), and Na_2O (up to 0.19 wt.%) (Figure 7; Table 2; Supplementary Materials).

Sometimes, oscillatory zoning was observed for small crystals and rims of the large ones with Mg# = 77.7–85.6 in the cores and 72.3–87.5 on the periphery (Figure 6b,e,h). In the groundmass, clinopyroxene formed microphenocrysts or microlites with a low Mg# 81.8–50.3 (Figure 7; Supplementary Materials). They were composed of augite and diopside ($En_{27–49}Wo_{29–50}Fs_{10–26}$) (Figure 7a). Compositions of clinopyroxene from the groundmass were generally close to the rims of the phenocrysts and showed a wide range of Al_2O_3 content (0.70–7.48 wt.%), high contents of TiO_2 (up to 1.55 wt.%) and Na_2O (up to 0.53 wt.%), and a lower content of Cr_2O_3, not exceeding 0.32 wt.% (Figure 7).

Variations in the Al_2O_3 content with Mg# in the clinopyroxenes generally showed a main trend of a pronounced increase in Al_2O_3 content from the cores to the rims of the phenocrysts, followed by a decrease in the groundmass microlites (Figure 7c,d). This variation may indicate the existence of an enrichment melt with Al and the subsequent addition of plagioclase to the olivine–clinopyroxene cotectic. However, some samples did not show significant accumulation of alumina (Figure 7c,d).

In the Barangol Complex intrusions, clinopyroxene formed either euhedral crystals (2–8 mm) or anhedral grains (Figures 3 and 6c,f). Clinopyroxene generally did not have zoning, except in grains from the Choburak gabbro (Figures 3 and 6c,f). Clinopyroxene from these rocks also corresponded mainly to diopside ($En_{31–48}Wo_{44–48}Fs_{5–24}$) (Figure 7b; Table 2; Supplementary Materials).
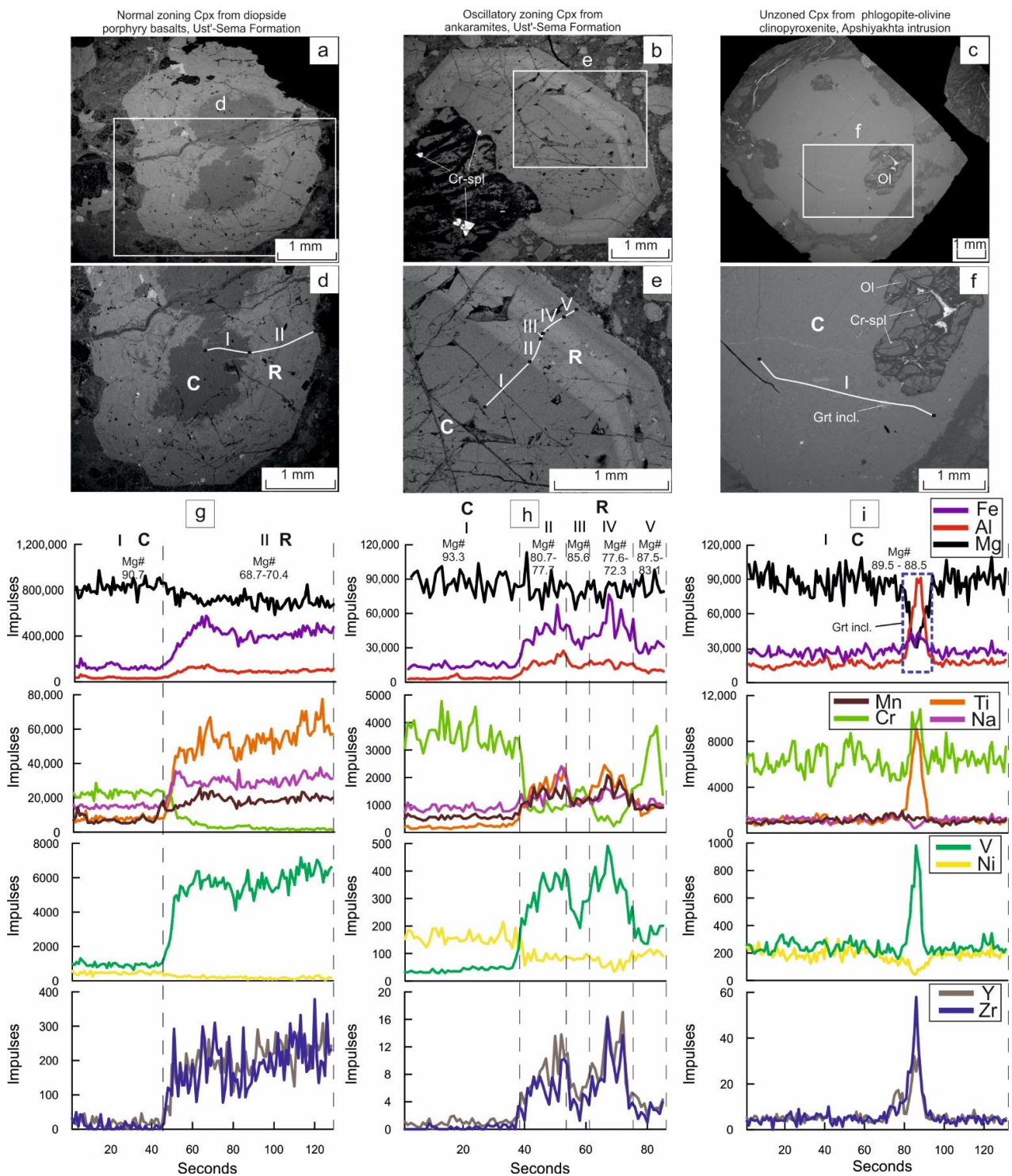
Figure 6. Zoning clinopyroxene crystals from the Ust'-Sema Formation and the Barangol Complex rocks, Gorny Altai: (**a–c**) back-scattered electron (BSE) images of clinopyroxene crystals (general view); (**d–f**) back-scattered electron (BSE) images of enlarged rims, and the lines indicate the laser beam path; (**g–i**) variations of major- and trace-elements using LA-ICP-MS (pulses per second). Mg# in the diagrams used are from the SEM EDS. The pronounced peak in diagram (i) is a result of the existence of a secondary Ca–garnet inclusion (Grt incl). C—core; R—rim.
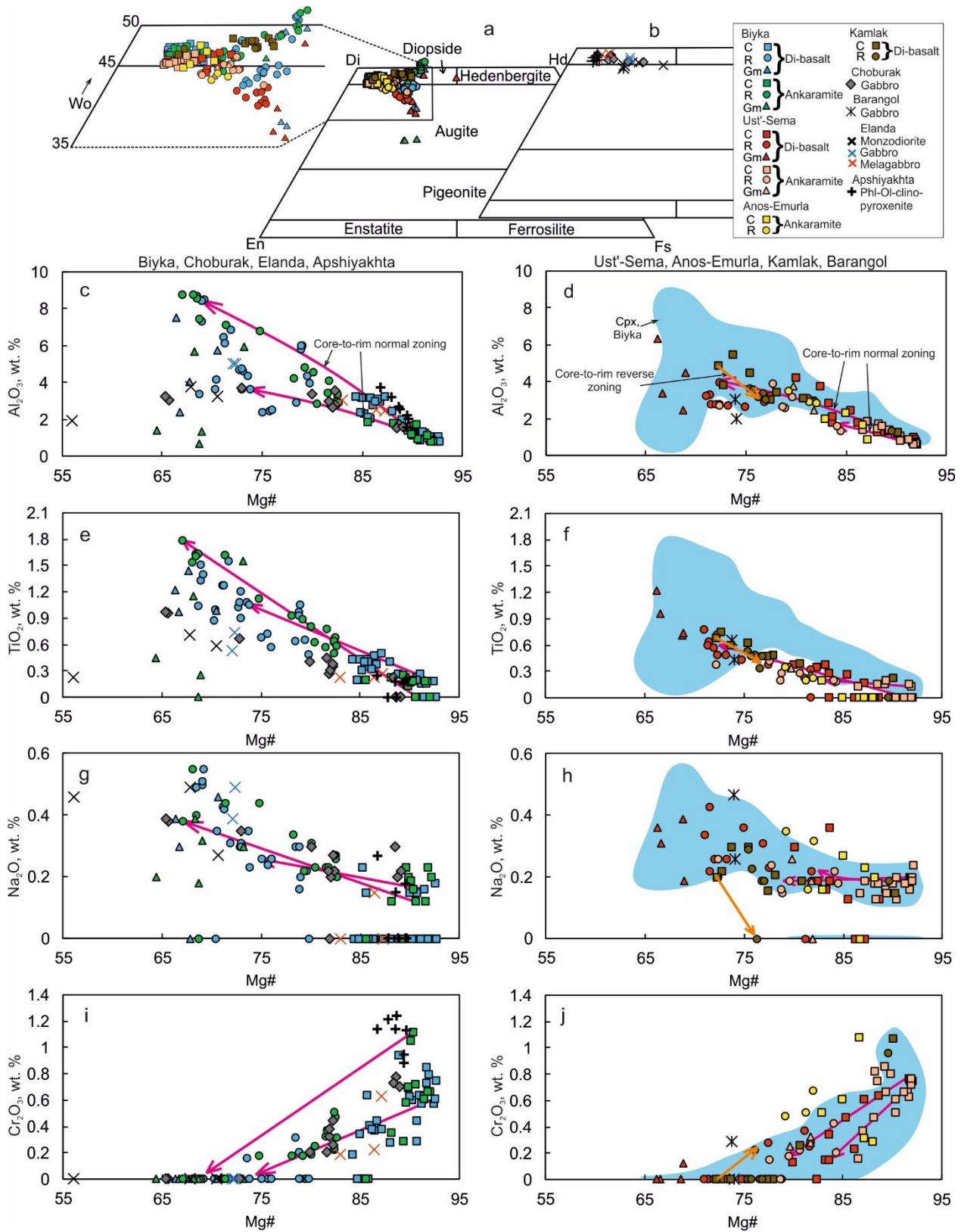
Figure 7. Compositions of clinopyroxene from the Ust'-Sema Formation and Barangol Complex rocks, Gorny Altai: (**a**,**b**) classification diagram [27] for pyroxenes from the Ust'-Sema Formation (**a**) and the Barangol Complex (**b**) [27]; (**c**–**j**) variations in Mg# with Al_2O_3, TiO_2, Na_2O, and Cr_2O_3 for clinopyroxene. For zoning clinopyroxene phenocrysts: C—core; R—rim; Gm—from the groundmass. Trends show typical cases of normal (purple) and reverse (orange) zoning.

Mg# for clinopyroxene varied from 89.6 to 83.0 in the phlogopite–olivine clinopyroxenite (Apshiyakhta) and melagabbro (Elanda) to 74.1–56.0 in gabbro and monzodiorite (Elanda) and gabbro (Barangol) (Figure 7; Table 2; Supplementary Materials). For clinopyroxene of Choburak gabbro, the cores of crystals had a high Mg# 89.1–81.7, where the rims had a low Mg# 80.0–65.4 (Figure 7; Table 2; Supplementary Materials).

The clinopyroxene from the Apshiyakhta intrusion had the highest content of Cr_2O_3 (0.88–1.24 wt.%) compared to Cr_2O_3 < 0.77 wt.% for clinopyroxene from the rocks of Elanda, Barangol, and Choburak (Figure 7; Table 2). The clinopyroxene of the Apshiyakhta intrusion, the melagabbro of the Elanda intrusion, and Choburak gabbro (cores) were characterized by low contents of Al_2O_3 (1.55–3.76 wt.%), TiO_2 (up to 0.45 wt.%), and Na_2O (up to 0.30 wt.%), and high contents of Cr_2O_3 (up to 1.24 wt.%, with an average 0.70 wt.%) and CaO (22.33–24.57 wt.%) (Figure 7; Table 2).

In contrast, clinopyroxene from Elanda gabbro and monzodiorite, gabbro of the Barangol intrusion and Choburak (rims of crystals) had high contents of Al_2O_3 (1.95–4.99 wt.%), TiO_2 (up to 0.73 wt.%), and Na_2O (up to 0.49 wt.%), and low contents of Cr_2O_3 (up to 0.29 wt.%) and CaO (21.20–22.50 wt.%) (Figure 7; Table 2).

The results from the LA-ICP-MS profiles showed that the cores had higher contents of Mg, Cr, Ni, and Ca, and lower contents of Fe, Al, Ti, Na, Mn, V, Y, and Zr; and the rims vice versa (Figure 6g,h).

Therefore, the compositions of clinopyroxene from both the Ust'-Sema Formation volcanic rocks and the Barangol Complex intrusions showed a negative correlation of Mg# with the contents of TiO_2, Al_2O_3, and Na_2O and a positive correlation with the content of Cr_2O_3 (Figure 7).

The clinopyroxene compositions from phlogopite–olivine clinopyroxenite of the Apshiyakhta intrusion, Elanda melagabbro, and Choburak gabbro (crystal cores) were similar to the compositions of the cores of clinopyroxene phenocrysts from the Ust'-Sema volcanic rocks. While the clinopyroxene compositions from the Elanda intrusion gabbro and monzodiorite, Barangol gabbro, and the Choburak (crystal rims) were similar to the compositions of the rims of the clinopyroxene phenocrysts and microlites of the Ust'-Sema volcanic rocks (Figure 7).

4.3.2. Plagioclase

Plagioclase is the main rock-forming mineral for the diopside porphyry basalts of the Ust'-Sema Formation. It forms microphenocrysts (up to 1 mm) or microlites (Figure 2b,d). Most of the plagioclase is saussuritized. In the preserved relics, it was represented by bytownite and labradorite An_{49-71} (Figure 2b,d; Table 3). In the groundmass, basic plagioclase was also represented by bytownite–labradorite An_{59-77} (Table 3). It should be noted that in the ankaramites from the Biyka and the Ust'-Sema volcanoes, plagioclase was present only as microlites in the groundmass and represented by labradorite An_{50-69} (Table 3). However, in the Anos-Emurla ankaramites, it was completely absent.

In the Barangol Complex intrusions, plagioclase was also strongly altered, and in the preserved grains from the Elanda gabbro and melagabbro, it was represented by andesine–oligoclase (Figure 3; Table 3).

4.3.3. Olivine

Gibsher et al. [4] reported very rare findings of olivine in the Ust'-Sema Formation rocks. Unfortunately, unaltered olivine was not found in our samples, only very rare microphenocrysts (up to 1 mm) of what is believed to be altered olivine (up to 1–2 vol.%) were observed in diopside porphyry basalts of the Biyka volcanic edifice. Grains were completely replaced by an aggregate of chlorite, epidote, and magnetite. Olivine (Fo_{83-86}, Table 4) was well-preserved in phlogopite–olivine clinopyroxenite of the Apshiyakhta intrusion as large idiomorphic crystals (1–6 mm in diameter) or inclusions in clinopyroxene (Figures 3f and 6c,f). It is characterized by moderate contents of CaO (up to 0.29 wt.%) and NiO (0.20–0.41 wt.%) (Table 4).

Table 3. Major element composition (by SEM-EDS) of plagioclase from the Ust'-Sema Formation and the Barangol Complex rocks, Gorny Altai.

Analysis	SiO$_2$	Al$_2$O$_3$	FeO	CaO	Na$_2$O	K$_2$O	Total	An
1	50.53	31.06	1.40	14.16	3.24	0.39	100.78	69.2
2	54.20	28.90	0.58	9.88	4.81	0.90	99.27	50.3
3	48.71	31.72	1.12	15.62	2.60	<dl	99.77	76.9
4	52.24	29.34	0.99	12.48	4.26	0.29	99.61	60.8
5	52.20	28.57	1.48	12.13	4.37	0.45	99.19	59.0
6	51.45	29.63	1.33	13.39	3.63	0.36	99.78	65.7
7	54.87	28.88	0.58	9.73	4.84	1.11	100.01	49.1
8	50.30	25.87	2.28	17.25	3.61	0.41	100.00	71.1
9	57.63	26.70	0.48	8.51	6.61	0.58	100.50	40.2
10	61.27	24.83	0.37	2.88	8.09	2.40	99.84	14.2

Plagioclase from (1–2) ankaramites; (3–8) diopside porphyry basalts; (9–10) Elanda intrusion: (9) gabbro and (10) melagabbro. (<dl)—below detection limit.

4.3.4. Amphibole

In the Ust'-Sema Formation volcanic rocks, amphibole was found in several samples of the diopside porphyry basalts from the Biyka volcanic edifice (up to 5 vol.%). Amphibole formed microphenocrysts (0.1–0.7 mm, rarely up to 2 mm) of euhedral prismatic shape or anhedral grains. The composition of amphibole from the diopside porphyry basalts was represented by magnesian hastingsite and tschermakite [10,28]. Mg# varied from 82.4–83.2 in magnesio–hornblende to 56.3–70.0 in tschermakite and 55.7–68.2 in magnesian hastingsite. The TiO$_2$ content was 2.32–3.97 wt.% in magnesian hastingsite and tschermakite.

Low-Ti magnesian hastingsite was found in the Elanda melagabbro as anhedral grains (Figure 3c) with a low Mg# 44.4–46.4 and a relatively low content of TiO$_2$ (1.25–1.52 wt.%).

Table 4. Major element composition (by SEM-EDS) of olivine from of the Apshiyakhta intrusion phlogopite–olivine clinopyroxenite (Barangol Complex), Gorny Altai.

Analysis	SiO$_2$	FeO	MnO	MgO	CaO	NiO	Total	Fo
1	39.62	13.21	<dl	46.37	<dl	0.36	99.56	86.2
2	39.11	13.25	0.25	45.72	<dl	0.41	98.73	86.0
3	39.30	15.18	0.25	44.74	0.13	0.25	99.85	84.0
4	40.20	15.46	0.34	45.27	0.14	0.33	101.74	83.9
5	39.86	15.94	0.26	44.97	0.00	0.20	101.23	83.4
6	39.19	15.34	0.22	45.19	0.13	0.29	100.35	84.0
7	39.79	15.89	0.28	45.42	0.13	0.28	101.79	83.6
8	40.22	14.61	0.28	46.27	0.29	0.24	101.92	85.0
9	39.77	14.37	0.31	46.23	0.22	0.32	101.23	85.2
10	38.72	14.42	0.28	44.59	0.10	0.31	98.42	84.6
11	39.60	14.40	0.34	45.47	0.15	0.27	100.22	84.9

(1–7) Crystals; (8–11) inclusions in clinopyroxene. (<dl)—below detection limit.

4.3.5. Cr-Spinel and Magnetite

Cr-spinel formed a fine inclusion (5–100 μm, rarely up to 200 μm) in the high-Mg clinopyroxene (Mg# 71.4–92.8) from the Ust'-Sema Formation volcanic rocks, the Choburak gabbro, and Apshiyakhta phlogopite–olivine clinopyroxenite (Table 5). Some inclusions of Cr-spinel (10–400 μm) were observed in olivine (Fo 83.9–84.9) grains from phlogopite–olivine clinopyroxenite of the Apshiyakhta intrusion (Table 5). Cr-spinel was also found as individual grains (15–200 μm) in the groundmass from the Kamlak unit diopside porphyry basalts or in altered clinopyroxene from Ust'-Sema diopside porphyry basalts and Choburak gabbro (Figure 6b; Table 5).

Cr-spinel from the Ust'-Sema Formation volcanic rocks was represented by chromite and magnesiochromite, where the Cr-spinel from the Choburak gabbro was chromite (Figure 8a). They were characterized by high Cr# 75.6–88.1 and Mg# 33.9–69.2 and a low

Fe# 7.1–19.6 (Table 5). The Cr-spinel content of TiO_2 varied from 0.13–0.68 wt.% in the rocks of the Ust'-Sema volcanic edifice, the Kamlak unit, and the Choburak gabbro to 0.87–0.97 wt.% in the Biyka volcanic edifice rocks (Table 5). The Al_2O_3 content varied in the range of 5.31–10.43 wt.% (Figure 8b; Table 5).
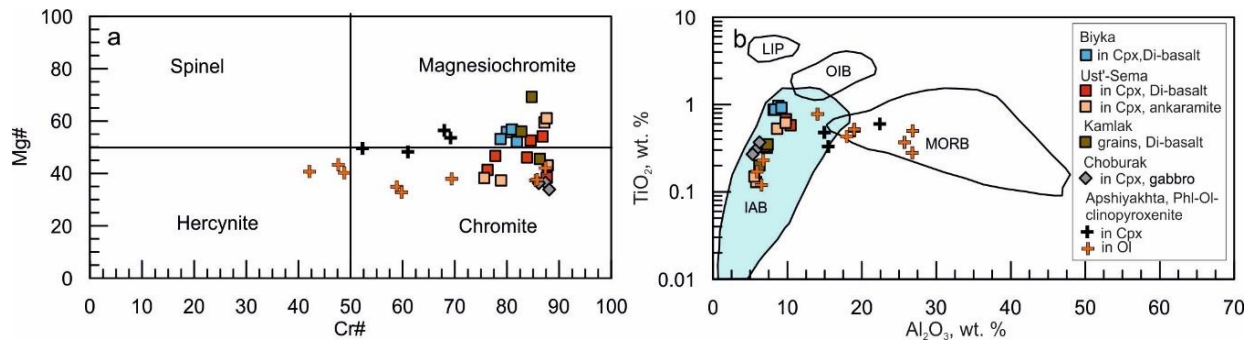

Figure 8. (**a**) Classification diagram for spinels [29]; (**b**) Al_2O_3 versus TiO_2 discrimination diagram for spinels from different tectonic settings [30]. IABs—island-arc basalts; OIBs—ocean island basalts; MORBs—mid-ocean ridge basalts; LIPs—basalts of large igneous provinces.

Cr-spinel from Apshiyakhta phlogopite–olivine clinopyroxenite had a diverse composition and was represented by chromite, magnesiochromite, and hercynite (Figure 8a). Inclusions of Cr-spinel in clinopyroxenes in these rocks had a relatively low Cr# 52.3–69.2 and a high Mg# 48.3–56.4 versus Cr# 42.1–87.4 and Mg# 32.8–43.4 for inclusions in olivine (Table 5). The TiO_2 content of Cr-spinel inclusions varied from 0.33–0.60 wt.% in clinopyroxenes to 0.12–0.78 wt.% in olivine (Table 5). The Al_2O_3 content reached up to 26.81 wt.% (Figure 8b; Table 5). The points of the Cr-spinel compositions from the volcanic rocks of the Ust'-Sema Formation and the Choburak gabbro fall into the field of island arc systems, whereas the Cr-spinel from phlogopite–olivine clinopyroxenite of the Apshiyakhta intrusion were shifted toward the field of mid-ocean ridge assemblages (Figure 8b).

Magnetite is common as inclusions (10–200 μm) in the cores of clinopyroxene phenocrysts in the Ust'-Sema Formation volcanics. Rarely it occurs as microcrystals (50–300 μm) in the groundmass in the ankaramites of the Anos-Emurla volcanic edifice (Table 5).

4.4. Trace Elements in Clinopyroxene

Chondrite-normalized rare-earth element patterns for the clinopyroxenes from the Ust'-Sema Formation and the Barangol Complex rocks generally showed a slight depletion in light rare-earth element $(La/Yb)_N$ = 0.1–1.0 (with an average 0.4) (Figure 9a,c,e,g; Table 2; Supplementary Materials) versus <0.05 in subduction-associated peridotites [31]. REE concentrations in clinopyroxene phenocrysts from the volcanic rocks showed a clear negative correlation with Mg#. In other words, the cores had a lower concentration of REE than the rims (Figure 9a,c,e; Table 2; Supplementary Materials).

The concentrations of the REE in the clinopyroxene phenocrysts from ankaramites were similar to those in diopside porphyry basalts (Figure 9). However, some analyses from the rims of clinopyroxene phenocrysts from the Biyka volcanic edifice, unlike the other areas, were characterized by a clear enrichment in REE $(La/Yb)_N$ = 1.1–1.7 (1.4 on average) (Figure 9, Table 2; Supplementary Materials). These features were also observed during the study of the major elements in the clinopyroxenes (Figure 7).

The REE concentrations in clinopyroxenes from the Barangol Complex were negatively correlated with Mg# (Figure 9a,c,e,g; Table 2; Supplementary Materials). The clinopyroxenes from the phlogopite–olivine clinopyroxenite (Apshiyakhta), melagabbro (Elanda), and gabbro (Choburak) had lower REE concentrations than the Elanda gabbro and monzodiorite and the Barangol gabbro (Figure 9a,c,e,g; Table 2; Supplementary Materials). Europium anomalies for all the studied clinopyroxenes, both from the Ust'-Sema Formation and

Barangol Complex rocks, were either absent or slightly varied from positive to negative (Eu/Eu* = 0.4–1.9, on average 1.0) (Table 2; Supplementary Materials).

Table 5. Major element composition (by SEM-EDS) of Cr-spinel and magnetite from the Ust'-Sema Formation and the Barangol Complex rocks, Gorny Altai.

Analysis	TiO₂	Al₂O₃	Cr₂O₃	FeO *	Fe₂O₃ *	MgO	Total	Cr#	Mg#	Fe#	Mg#$_{Cpx}$, Fo$_{Ol}$	Note
1	0.13	5.78	58.67	14.41	9.19	11.54	99.80	87.2	59.5	11.2	92.8 (Mg#)	Cr-spl
2	0.15	5.56	58.43	13.67	9.54	11.67	99.42	87.6	61.1	11.7	92.8 (Mg#)	Cr-spl
3	0.53	8.62	47.93	22.61	14.26	7.21	100.22	78.9	37.3	17.6	82.7 (Mg#)	Cr-spl
4	0.62	9.75	45.09	22.69	16.14	7.50	100.56	75.6	38.3	19.6	82.7 (Mg#)	Cr-spl
5	<dl	5.48	58.74	20.35	8.25	8.41	100.40	87.8	43.1	10.3	89.1 (Mg#)	Cr-spl
6	0.32	7.24	56.04	19.60	9.12	9.14	100.82	83.8	46.1	11.2	91.8 (Mg#)	Cr-spl
7	0.33	6.92	56.37	17.64	9.94	10.63	100.84	84.5	52.6	12.1	90.7 (Mg#)	Cr-spl
8	0.58	10.43	49.93	21.94	10.81	8.37	100.98	76.3	41.3	13.2	altered Cpx	Cr-spl
9	0.68	9.81	51.17	19.88	9.78	9.45	99.79	77.8	46.7	12.1	altered Cpx	Cr-spl
10	<dl	6.29	61.80	16.77	5.79	10.93	100.99	86.8	54.2	7.1	altered Cpx	Cr-spl
11	<dl	5.69	60.09	21.87	6.27	7.50	100.77	87.6	38.4	7.9	altered Cpx	Cr-spl
12	0.87	8.12	54.78	17.86	8.77	10.58	100.75	81.9	52.1	10.8	90.8 (Mg#)	Cr-spl
13	0.97	8.77	52.27	16.53	10.34	11.33	99.68	80.0	55.8	12.7	90.4 (Mg#)	Cr-spl
14	0.88	8.31	52.62	15.81	10.56	11.29	99.51	80.9	56.8	13.0	90.4 (Mg#)	Cr-spl
15	0.92	9.20	50.92	17.10	10.38	10.53	98.89	78.8	53.2	12.9	90.4 (Mg#)	Cr-spl
16	0.20	6.22	58.42	19.88	6.41	9.12	101.01	86.3	45.5	8.1	Gm	Cr-spl
17	0.00	8.24	58.84	15.31	7.15	10.68	103.33	82.7	56.0	8.6	Gm	Cr-spl
18	0.35	7.33	60.60	11.97	7.40	14.74	102.26	84.7	69.2	8.8	Gm	Cr-spl
19	0.30	5.71	58.77	22.72	5.77	7.20	100.15	87.4	36.5	7.4	71.4 (Mg#)	Cr-spl
20	0.37	6.25	57.81	22.97	6.26	7.18	100.44	86.1	36.3	8.0	71.4 (Mg#)	Cr-spl
21	0.27	5.31	58.76	23.48	5.93	6.62	100.02	88.1	33.9	7.7	altered Cpx	Cr-spl
22	0.60	22.41	36.61	19.61	10.32	10.46	99.41	52.3	49.6	12.0	86.8 (Mg#)	Cr-spl
23	0.48	14.96	50.13	17.46	5.05	11.14	99.16	69.2	53.6	6.2	89.8 (Mg#)	Cr-spl
24	0.50	18.95	44.17	19.76	7.17	10.12	100.76	61.0	48.3	8.5	89.7 (Mg#)	Cr-spl
25	0.33	15.49	49.01	16.28	6.76	11.56	99.90	68.0	56.4	8.0	90.1 (Mg#)	Cr-spl
26	0.78	14.04	47.34	23.21	8.20	7.76	101.05	69.4	37.9	10.0	84.9 (Fo)	Cr-spl
27	0.23	6.76	59.38	21.82	4.46	7.20	100.02	85.5	37.4	5.7	84.9 (Fo)	Cr-spl
28	0.17	5.93	61.36	20.29	3.79	8.16	99.66	87.4	42.0	4.8	84.9 (Fo)	Cr-spl
29	0.12	6.52	58.71	21.67	4.42	7.23	99.54	85.8	37.6	5.7	84.9 (Fo)	Cr-spl
30	0.37	25.73	36.54	22.98	5.49	8.54	99.97	48.8	40.2	6.4	83.9 (Fo)	Cr-spl
31	0.50	26.81	36.39	21.30	5.05	9.00	99.59	47.7	43.4	5.9	83.9 (Fo)	Cr-spl
32	0.52	18.97	40.46	24.87	9.55	7.28	100.95	58.9	34.9	11.4	84.0 (Fo)	Cr-spl
33	0.43	17.97	39.83	25.12	10.73	6.63	100.34	59.8	32.8	12.9	84.0 (Fo)	Cr-spl
34	0.28	26.77	29.04	23.12	11.52	8.59	98.49	42.1	40.6	13.3	84.0 (Fo)	Cr-spl
35	2.12	<dl	3.39	32.92	60.02	<dl	93.57	nc	nc	nc	80.1 (Mg#)	Mag
36	1.12	<dl	3.38	33.36	63.74	<dl	95.65	nc	nc	nc	Gm	Mag
37	4.35	<dl	2.12	36.52	58.92	<dl	96.49	nc	nc	nc	Gm	Mag
38	4.32	<dl	1.67	35.74	59.35	<dl	95.90	nc	nc	nc	Gm	Mag
39	<dl	2.40	34.76	27.45	31.46	<dl	99.40	nc	nc	nc	Gm	Mag
40	<dl	1.59	30.63	27.48	36.57	<dl	98.61	nc	nc	nc	Gm	Mag

(1–34) Cr-spinel: (1–5) from ankaramites; (6–18) from diopside porphyry basalts; (19–21) from the Choburak gabbro; (22–34) from phlogopite–olivine clinopyroxenite of the Apshiyakhta intrusion; (35–40) magnetite from ankaramites. (<dl)—below detection limits. nc—not calculated; * the contents of FeO and Fe₂O₃ were calculated from the total content of FeO, based on the stoichiometric considerations. Mg# = 100 (Mg/(Mg + Fe^{+2}); Cr# = 100 Cr/(Cr + Al); Fe# = 100 Fe^{+3}/(Fe^{+3} + Al + Cr). Mg#$_{Cpx}$—Fo$_{Ol}$ hostess. Cr-spl—Cr-spinel; Mag—magnetite; Gm—microcrystals in groundmass.

Multiple trace element patterns, normalized to the primitive mantle [32], also clearly showed common features for all clinopyroxenes from the Ust'-Sema Formation and Barangol Complex rocks (Figure 9b,d,f,h). Negative anomalies were observed for high-field-strength elements (Zr, Hf, Nb, and Ti) and large-ion lithophile elements (Rb) (Figures 9b,d,f,h and 10; Table 2; Supplementary Materials). However, some clinopyroxenes from volcanic rocks of the Biyka volcanic edifice were characterized by a positive anomaly in Ti ((Ti/Gd)$_{PM}$ =

1.0–2.4) (Figures 9 and 10; Table 2; Supplementary Materials). Sr showed a positive anomaly in the high-Mg clinopyroxenes and a negative anomaly in the low-Mg ones (Figure 10b; Table 2; Supplementary Materials).
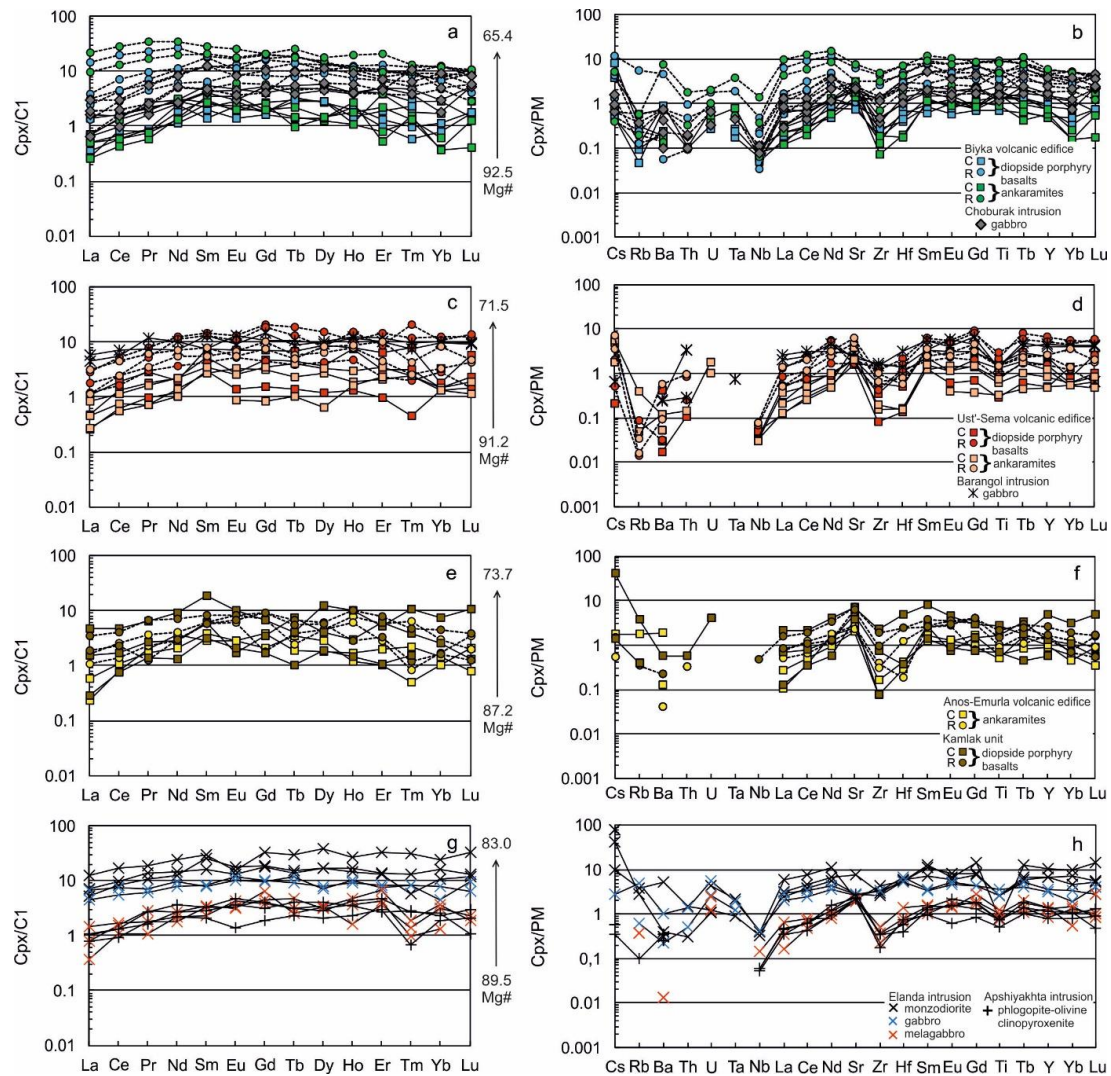

Figure 9. (**a**,**c**,**e**,**g**) Chondrite-normalized rare-earth element patterns [26] and (**b**,**d**,**f**,**h**) multiple trace element patterns normalized to the primitive mantle [32] for the clinopyroxenes from the rocks of the Ust'-Sema Formation and the Barangol Complex.
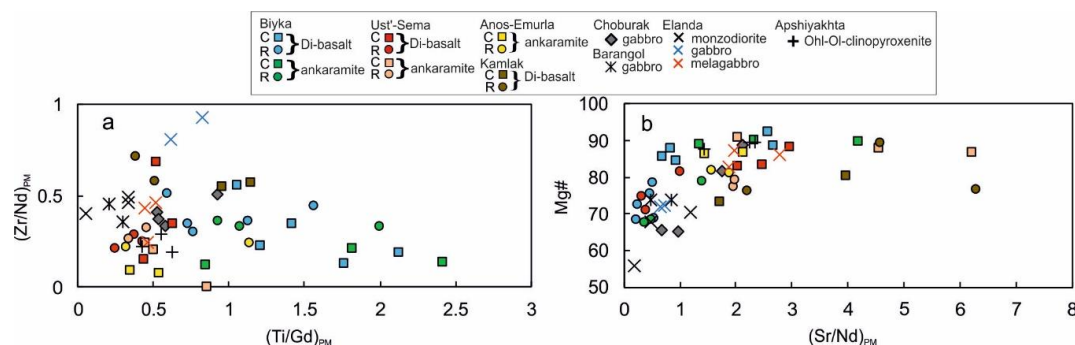

Figure 10. (**a**) (Ti/Gd)$_{PM}$ verses (Zr/Nd)$_{PM}$; (**b**) (Sr/Nd)$_{PM}$ verses Mg# for the clinopyroxenes from the rocks of the Ust'-Sema Formation and the Barangol Complex. All ratios were normalized to the primitive mantle [32].

5. Discussion

The Ust'-Sema volcanics and Barangol Complex rocks have specific distinctive features. First of all, the high content of diopside pyroxene, which has been paid attention to by all previous researchers [1,4,6–10]. The reason for this is both the high content of calcium in the parental melts, which was confirmed by the study of melt inclusions [1,7], and the possibility for phenocryst accumulation in some portions of magma or even in separate flows.

Clinopyroxene in effusive rocks is quite resistant to alteration, and its chemical composition is widely used to determine the geodynamic setting and, consequently, the composition and nature of the melt source [11–18]. On the triple diagram TiO_2-SiO_2/100-Na_2O [13], points of clinopyroxene composition from the Ust'-Sema effusive rocks and Barangol Complex intrusions mainly fall into the fields of island arcs ankaramites and tholeiites. (Figure 11). However, a significant number of clinopyroxene compositions (mainly from the phenocryst rims) from the Biyka edifice and the Kuyus area were shifted to the typical MORB and OIB fields. Nevertheless, the cores of these crystals were no different from those typical of other areas.
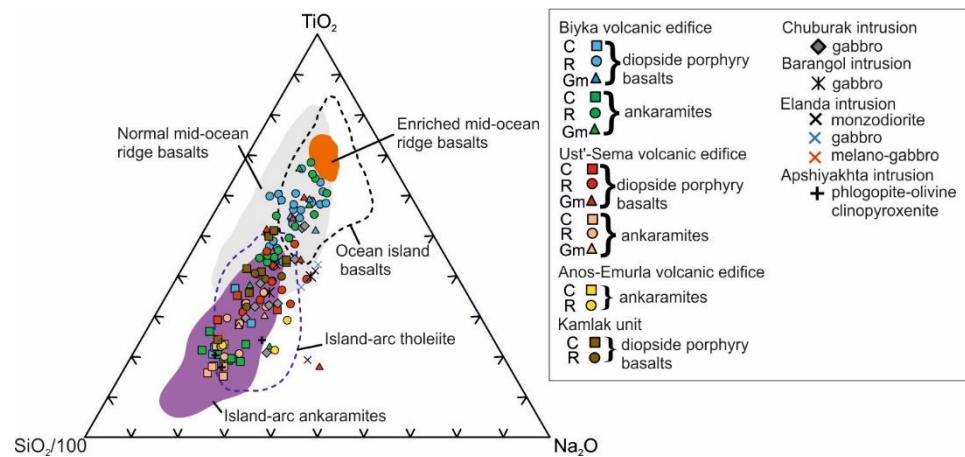
Figure 11. TiO_2-SiO_2/100–Na_2O (wt.%) discriminating diagram [13] for clinopyroxene from the Ust'-Sema Formation and the Barangol Complex rocks. The island arc ankaramites field is according to [33–36] and other fields are according to [13].

Distinctive features of clinopyroxene from some Biyka rocks and the Kuyus area include the high contents of TiO_2 and Al_2O_3 and the moderate enrichment of light REE (Figures 7 and 9). A high TiO_2 content was also characteristic for these rocks' bulk compositions (Figure 5e). These features are likely related to the fact that the Ust'-Sema Formation volcanics in this area overlap are an older Manzherok Formation of an OIB-type intraplate volcano (seamount). There was undoubtedly a hiatus between the end of the OIB-type volcanism and ankaramitic volcanism beginning, during which, at least, a significant part of the guyot carbonate cap (Cheposh Formation) was formed [8]. However, its duration has not been reliably established and is debatable. It is possible that at the upper levels of the plumbing system feeding volcanoes, the ankaramite magma either interacted with high-Ti basalts and gabbroids, which formed during the crystallization of magma of the Manzherok magma chambers, or even mixed with some portion of the OIB-type melt. In any case, this interaction did not take place in a deep magma source but at higher levels—that is, in the crust.

A dramatic difference in the texture and chemical composition of the clinopyroxene cores and rims in most grains, as well as frequent signs of the cores' partial dissolution, indicate an abrupt change in PTx conditions in the magmatic system. Various authors, based on the allocation of clinopyroxenes compositional groups, propose the identification of a series of different magmatic reservoirs or suggest that the magmatic abrasion resulted in adding into the magma of some clinopyroxene grains from the paragenesis of lover-crust

granulites or lithospheric mantle [15,16]. Pressure estimates for our data set from single-clinopyroxene geobarometers [37,38] show inconsistent values that contradict geological data, mainly due to the elevated levels of Al and Na in the rims. For cores, the pressure estimates ranged mainly from 4 to 9 kbar.

Gibsher et al. [4] suggested that the source of green chromium-bearing diopside cores are mantle peridotites. The comparison to the clinopyroxene compositions from the typical subduction-zone lherzolite from the Kamchatsky Mys [31] confirms that the Ust'-Sema clinopyroxene cores were crystallized from the basaltic melt and were not from mantle paragenesis, considering that the clinopyroxenes from mantle lherzolite were strongly depleted on the light REE and characterized by negative Sr anomalies (Figure 9). Moreover, general similarities were observed when compared to the clinopyroxene composition from non-mantle rocks, for example, ankaramites of island arcs [33] (Figure 9).

The trace element composition of the clinopyroxene phenocrysts cores from the rocks of the Ust'-Sema Formation coincides with the composition of the clinopyroxenes from phlogopite-olivine clinopyroxenite of the Apshiyakhta intrusion, melagabbro of the Elanda intrusion, and Choburak gabbro (Figures 9 and 10; Table 2). The rims, meanwhile, coincided with the composition of the clinopyroxene from gabbro and monzodiorite of the Elanda intrusion, and gabbro of the Barangol intrusion (Figures 9 and 10; Table 2).

Thus, the clinopyroxenes from the Ust'-Sema Formation and the Barangol Complex rocks have common geochemical features: the same chondrite-normalized REE spectrum distribution; negative correlation rare and rare-earth element concentrations with Mg#; negative anomalies in high-field-strength elements (Zr, Hf, Nb, and Ti) and large-ion lithophile elements (Rb); Sr behavior with Mg# variability (Figures 9 and 10; Table 2).

Some models suggest that the differentiation of such a high-calcium melt in island arc-related magma chambers leads to the formation of Ural–Alaskan-type massifs [39,40]. From the point of mineralogical criteria, their ultramafic–mafic units were characterized by the abundance of high-calcium clinopyroxene and the absence of plagioclase and orthopyroxene as well as the high chromium content values in Cr-spinels [39,41–43]. The gabbro units also retain the high-calcium clinopyroxene's specificity. Such features are also observed in the Barangol Complex intrusions.

Common features also included high Mg# in clinopyroxene; negative correlations of Mg# with Ti, Al, and Na contents; positive correlations with Cr; uniform distribution spectra of rare-earth elements; spider diagrams with negative anomalies in Zr, Hf, Nb, Ti, and large ionic lithophilic elements (Ba), as well as coincidence with the trend of island arc cumulates (Figures 12 and 13).

On the $Al_{iv}*100/2$ and TiO_2 diagram and other binary plots (Figure 12), variations in the composition of clinopyroxene from rocks of the Ust'-Sema Formation coincided with the trend for island arc cumulates, which is typical for clinopyroxene from island arc ankaramites. At the same time, if we separately take the composition of clinopyroxenes from effusive rocks (basalts) of modern island arcs (for example, the Aleutian arc [44,45]), then variations in their composition take place in a much narrower range (Figure 12). However, the trace and REE spectra were very similar to each other (Figure 13).

The Cr-spinel from the Ust'-Sema and Barangol Complex intrusions was generally similar to the Ural–Alaskan ones with a slight difference in higher Cr# and Mg# and low contents of Al and Ti for some grains (Figure 14).
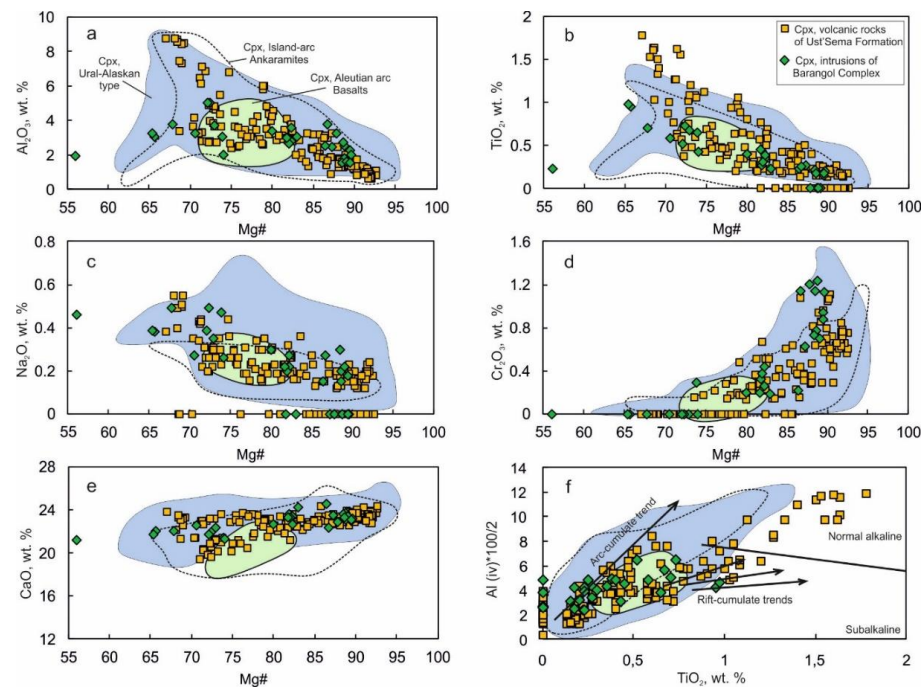
Figure 12. Variations in the composition of clinopyroxene from the rocks of the Ust'-Sema Formation and the Barangol Complex compared with clinopyroxene from island arc ankaramites [33–36], Ural–Alaskan-type intrusions [39,41,42], and basalts of the Aleutian arc [44,45]. (**a**) Mg# vs. Al_2O_3; (**b**) Mg# vs. TiO_2; (**c**) Mg# vs. Na_2O; (**d**) Mg# vs. Cr_2O_3; (**e**) Mg# vs. CaO (**f**) TiO_2 vs. Al_{iv}*100/2. The boundaries of the fields from [46] and the trends from [47].
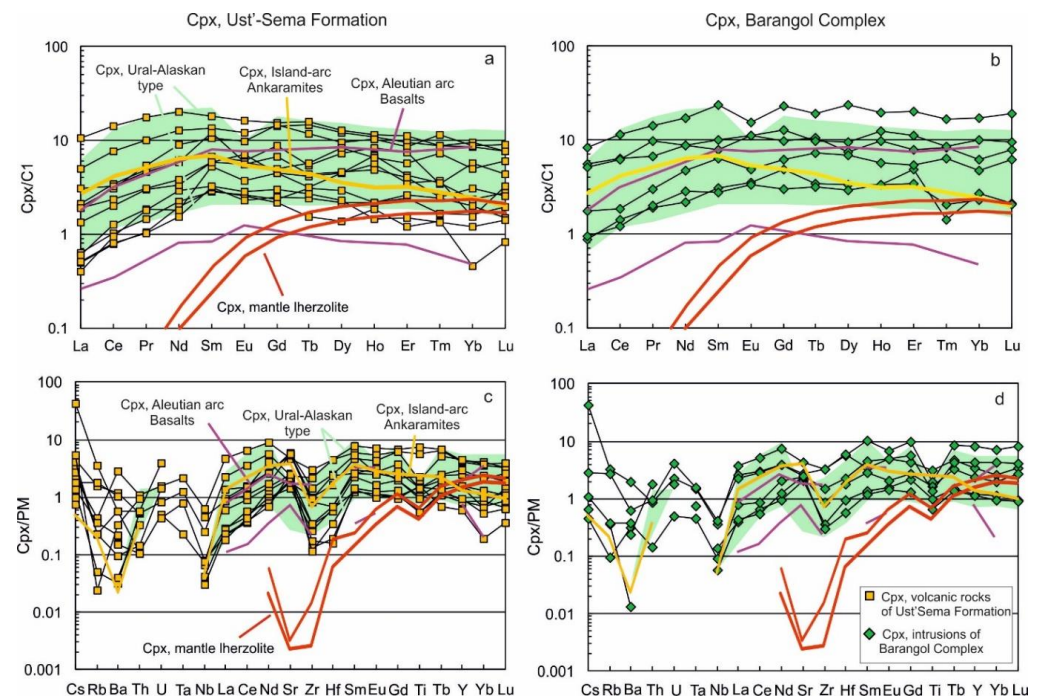

Figure 13. (**a**,**b**) Chondrite-normalized spectrum distribution of the rare-earth elements [26] and (**c**,**d**) primitive mantle-normalized spider diagrams [32] for the clinopyroxenes from the Ust'-Sema Formation and the Barangol Complex rocks compared with clinopyroxene compositions from island arc ankaramites [33] and mantle lherzolite of the Kamchatsky Mys [31] are shown. Continued line: core of crystal; dashed line: rim of crystal with clinopyroxene from island arc ankaramites [33], Ural–Alaskan-type intrusions [42], and basalts of the Aleutian arc [48].

In addition, it should be noted that in Uureg Nuur, Northwestern Mongolia, there is a similar-in-scale high-calcium magmatic association, also having an Early Cambrian age [49]. It is interesting that it is connected with local placer ferroplatinum mineralization [50], which style is typical for Ural–Alaskan-type ore systems.
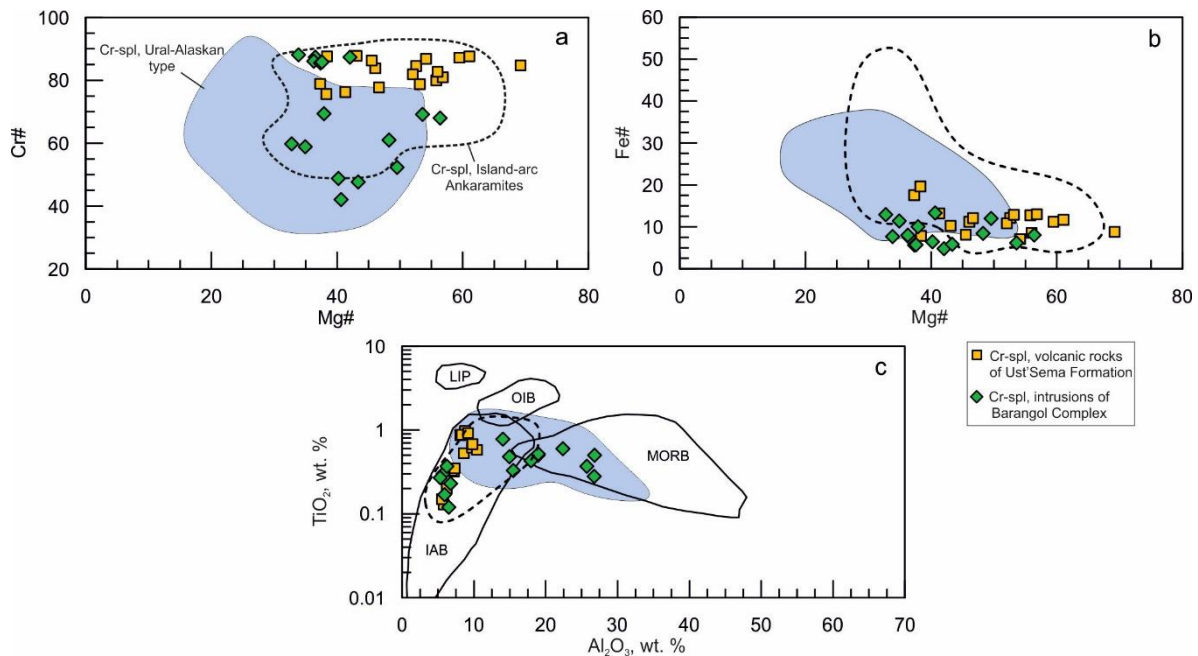
Figure 14. Variations in the composition of Cr-spinel from the rocks of the Ust'-Sema Formation and the Barangol Complex compared with the compositions of Cr-spinel from island arcs ankaramites [34–36] and Ural–Alaskan-type intrusions [39,41,42]. (**a**) Mg# verses Cr#; (**b**) Mg# verses Fe#; (**c**) Al_2O_3 versus TiO_2 discrimination diagram of spinels from different tectonic settings [30]. IABs—island-arc basalts; OIBs—ocean island basalts; MORBs—mid-ocean ridge basalts; LIPs—basalts of large igneous provinces.

6. Conclusions

1. Middle Cambrian Ust'-Sema Formation ankaramites and high-calcium diopside basalts have a single origin and a uniform magmatic source. The ankaramites were characterized by high contents of MgO (8.27–14.34 wt.%), CaO (12.09–14.48 wt.%) and a high CaO/Al_2O_3 ratio (1.1–1.6). The diopside porphyry basalts had low contents of CaO (9.79–11.86 wt.%) and MgO (6.35–7.84 wt.%), a low CaO/Al_2O_3 ratio (0.6–0.8), and a higher content of Al_2O_3 (13.74–16.67 wt.%).
2. The Barangol Complex rocks were clinopyroxenite and gabbro and shared common features with the Ust'-Sema volcanic rocks, especially in the composition of clinopyroxene and Cr-spinel. These features are typical for subduction-related ankaramites worldwide and Ural–Alaskan-type intrusions.
3. The cores of clinopyroxene phenocrysts were represented only by diopside in all types of rocks. The cores' composition was characterized by increased Cr, Ni, and Mg contents. The cores sometimes have a complex structure with a large number of inclusions but, at the same time, are homogeneous in chemical composition, while the rims had a more variable composition and much fewer inclusions. The rims were characterized by higher Fe, Al, Na, Ti, Mn, V, and Zr contents. In areas with oscillatory zoning, the contents of these elements varied greatly, but they were always higher than in the cores.
4. LA-ICP-MS analysis of the clinopyroxenes from both volcanic and intrusion rocks showed slight depletion of light rare-earth elements; strong depletion in high-field-strength (Zr, Hf, and Nb) and large-ion lithophile (Rb) elements and positive Sr anomaly.

5. Major- and trace-element composition of the clinopyroxenes showed that the Ust'-Sema clinopyroxene cores were crystallized from the basaltic melt and were not from mantle paragenesis.

6. The increased contents of Ti and incompatible elements in the rims of diopside phenocrysts from the Biyka volcano indicate a possible interaction of ankaramite-style magmas with high Ti melts or contamination with OIB-type rocks.

Author Contributions: N.K. and A.V. wrote the paper with input from A.I. and M.C. and conducted a study of clinopyroxene grains using LA-ICP-MS. N.K. carried out the petrographic study, studied samples using SEM, and worked with literature and analytical data. All authors have read and agreed to the published version of the manuscript.

Conflicts of Interest: The authors declare no conflict of interest.

References

1. Buslov, M.M.; Berzin, N.A.; Dobretsov, N.L.; Simonov, V.A. *Geology and Tectonics of Gorny Altai*; UIGGM: Novosibirsk, Russia, 1993; p. 122.

2. Berzin, N.A.; Coleman, R.G.; Dobretsov, N.L.; Zonenshain, L.P.; Xiao, X.; Chang, E.Z. Geodynamic map of the western part of the Paleoasian Ocean. *Russ. Geol. Geophys.* **1994**, *35*, 8–28.

3. Buslov, M.M.; Saphonova, I.Y.; Watanabe, T.; Obut, O.T.; Fujiwara, Y.; Iwata, K.; Semakov, N.N.; Sugai, Y.; Smirnova, L.V.; Kazansky, A.Y.; et al. Evolution of the Paleo-Asian Ocean (Altai–Sayan Region, Central Asia) and collision of possible Gondwana-derived terranes with the southern marginal part of the Siberian continent. *Geosci. J.* **2001**, *5*, 203–224. [CrossRef]

4. Gibsher, A.S.; Esin, S.V.; Izokh, A.E.; Kireev, A.D.; Petrova, T.V. Cambrian diopside porphyry basalts of the Cheposh zone in Gorny Altai: A model for fractionation of hybrid magmas in intermediate magmatic chambers. *Russ. Geol. Geophys.* **1997**, *38*, 1789–1801.

5. Dobretsov, N.L.; Buslov, M.M.; Safonova, I.Y.; Kokh, D.A. Fragments of oceanic islands in the Kurai and Katun' accretionary wedges of Gorny Altai. *Russ. Geol. Geophys.* **2004**, *45*, 1381–1403.

6. Zybin, V.A. *Etalon of the Ust'-Sema Complex of Porphyric Basalts and Trachybasalts (Gorny Altai)*; SNIIGGiMS: Novosibirsk, Russia, 2006; p. 278. (In Russian)

7. Simonov, V.A.; Safonova, I.Y.; Kovyazin, S.V.; Kurganskaya, E.V. Physic-chemical petrogenetic parameters of basaltic units in the Katun Zone of Gorny Altay. *Litosfera* **2010**, *3*, 111–117. (In Russian)

8. Safonova, I.Y.; Buslov, M.M.; Simonov, V.A.; Izokh, A.E.; Komiya, T.; Kurganskaya, E.V.; Ohno, T. Geochemistry, petrogenesis and geodynamic origin of basalts from the Katun' accretionary complex of Gorny Altai (southwestern Siberia). *Russ. Geol. Geophys.* **2011**, *52*, 421–442. [CrossRef]

9. Kruk, N.N. Evolution Continental Crust and Granitoid Magmatism of Gorny Altai. Ph.D. Thesis, Sobolev Institute of Geology and Mineralogy, Novosibirsk, Russia, 2015. (In Russian)

10. Khlif, N.; Vishnevskiy, A.V.; Izokh, A.E. Ankaramites of Gorny Altai: Mineralogical, petrographic and petrochemical features of diopside porphyry basalts of the Ust'-Sema Formation. *Russ. Geol. Geophys.* **2020**, *61*, 250–267. [CrossRef]

11. Nisbet, E.G.; Pearce, J.A. Clinopyroxene composition in mafic lavas from different tectonic setting. *Contrib. Mineral. Petrol.* **1977**, *63*, 149–160. [CrossRef]

12. Leterrier, J.; Maury, R.C.; Thonon, P.; Girard, D.; Marchal, M. Clinopyroxene composition as a method of identification of the magmatic affinities of paleo-volcanic series. *Earth. Planet. Sci. Lett.* **1982**, *59*, 139–154. [CrossRef]

13. Beccaluva, L.; Macciotta, G.; Piccardo, G.B.; Zeda, O. Clinopyroxene composition of ophiolite basalts as petrogenetic indicator. *Chem. Geol.* **1989**, *77*, 165–182. [CrossRef]

14. Aparicio, A. Relationship between clinopyroxene composition and the formation environment of volcanic host rocks. *IUP J. Earth Sci.* **2010**, *4*, 1–11.

15. Jankovics, M.É.; Tarascák, Z.; Dobosi, G.; Embey-Isztin, A.; Batki, A.; Harangi, S.; Hauzenberger, C. Clinopyroxene with divers origin in alkali basalts from the western Pannonian Basin: Implications from trace element characteristics. *Lithos* **2016**, *262*, 120–134. [CrossRef]

16. Batki, A.; Pál-Molnár, E.; Jankovics, M.É.; Kerr, A.C.; Kiss, B.; Markl, G.; Heincz, A.; Harangi, S. Insights into the evolution of an alkaline magmatic system: An in situ trace element study of clinopyroxenes from the Ditrău Alkaline Massif, Romania. *Lithos* **2018**, *300–301*, 51–71. [CrossRef]

17. Zhang, Y.; Yu, K.; Qian, H. LA-ICP-MS analysis of clinopyroxenes in basaltic pyroclastic rocks from the Xisha Islands, Northwestern South China Sea. *Minerals* **2018**, *8*, 575. [CrossRef]

18. Ubide, T.; Caulfield, J.; Brandt, C.; Bussweiler, Y.; Mollo, S.; Stefano, F.D.; Nazzari, M.; Scarlato, P. Deep magma storage revealed by multi-method elemental mapping of clinopyroxene megacrysts at Stromboli volcano. *Front. Earth Sci.* **2019**, *7*, 239. [CrossRef]

19. Buslov, M.M.; Geng, H.; Travin, A.V.; Otgonbaatar, D.; Kulikova, A.V.; Chen, M.; Glorie, S.; Semakov, N.N.; Rubanova, E.S.; Abildaeva, M.A.; et al. Tectonics and geodynamics of Gorny Altai and adjacent structures of the Altai–Sayan Folded Area. *Russ. Geol. Geophys.* **2013**, *54*, 1250–1271. [CrossRef]

20. *State Geological Map of the Russian Federation, Scale 1: 1000 000*, 3rd ed.; Series Altai-Sayansk, Sheet M-45 (Gorno-Altaysk); VSEGEI: St. Petersburg, Russian, 2011; p. 567. (In Russian)

21. Shokalsky, S.P. *Correlation of Magmatic and Metamorphic Complexes of the Western Part of the Altai-SAYAN Folded Region*; GEO SB RAS: Novosibirsk, Russia, 2000; p. 188. (In Russian)

22. *State Geological Map of the Russian Federation, Scale 1: 200 000*, 2nd ed.; Series Altai, Sheet M-45-VIII (Shebalino); VSEGEI: St. Petersburg, Russia, 2013; p. 242. (In Russian)

23. Lavrent'ev, Y.G.; Karmanov, N.S.; Usova, L.V. Electron probe microanalysis of minerals: Microanalyzer or scanning electron microscope? *Russ. Geol. Geophys.* **2015**, *56*, 1154–1161. [CrossRef]

24. Della-Pasqua, F.N.; Varne, R. Primitive ankaramitic magmas in volcanic arcs: A melt inclusion approach. *Can. Mineral.* **1997**, *35*, 291–312.

25. Le Maitre, R.W. *Igneous Rocks a Classification and Glossary of Terms Recommendations of the International Union of Geological Sciences, Sub-Commission on the Systematics of Igneous Rocks*; Cambridge University Press: Cambridge, UK, 2002; 236p.

26. Boynton, W.V. *Cosmochemistry of the Rare Earth Elements: Meteorite Studies*; Henderson, P., Ed.; Rare Earth Element Geochemistry; Elsevier: Amsterdam, The Netherlands, 1984; pp. 63–114.

27. Morimoto, N. Nomenclature of Pyroxenes. *Mineral. Petrol.* **1988**, *39*, 55–76. [CrossRef]

28. Leake, B.E. Nomenclature of amphiboles: Additions and revisions to the International Mineralogical Association's amphibole nomenclature. *Eur. J. Mineral.* **2004**, *16*, 190–195. [CrossRef]

29. Schulze, D. Origins of chromian and aluminous spinel macrocrysts from kimberlites in southern Africa. *Can. Mineral.* **2001**, *39*, 361–376. [CrossRef]

30. Kamenetsky, V.S.; Crawford, A.J.; Meffre, S. Factors controlling the chemistry of magmatic spinel: An empirical study of associated olivine, Cr-spinel and melt inclusions from primitive rocks. *J. Petrol.* **2001**, *42*, 655–671. [CrossRef]

31. Batanova, V.G.; Lyaskovskaya, Z.E.; Savelieva, G.N.; Sobolev, A.V. Peridotites from the Kamchatsky Mys: Evidence of oceanic mantle melting near a hotspot. *Russ. Geol. Geophys.* **2014**, *55*, 1395–1403. [CrossRef]

32. Sun, S.S.; McDonough, W.F. Chemical and isotopic systematic of oceanic basalts: Implications for mantle composition and processes. In *Magmatism in Ocean Basins*; Sauders, A.D., Norry, M.J., Eds.; Geological Society London Special Publications: London, UK, 1989; pp. 313–345.

33. Marchev, P.; Georgiev, S.; Zajacz, Z.; Manetti, P.; Raicheva, R.; Von Quadt, A.; Tommasini, S. High-K ankaramitic melt inclusions and lavas in the Upper Cretaceous Eastern Srednogorie continental arc, Bulgaria: Implication for the genesis of arc shoshonites. *Lithos* **2009**, *113*, 228–245. [CrossRef]

34. Barasdell, M.; Berry, R.F. Origin and evolution of primitive island arc ankaramites from Western Epi, Vanuatu. *J. Petrol.* **1990**, *31*, 747–777. [CrossRef]

35. Della-Pasqua, F.N. Primitive ankaramitic magmas in volcanic arcs: Evidence from melt inclusions. Ph.D. Thesis, University of Tasmania, Tasmania, Australia, 1997.

36. Pushkarev, E.V.; Ryazancev, A.V.; Gottman, I.A. Ankaramites of Presakmara-Voznesenska zone of the Southern Urals- geological position and composition. In *Yearbook Russian Academy of Sciences, Ural Branch, Institute of Geology and Geochemistry*; IGG UB RAS: Yekaterinburg, Russia, 2017; Volume 164, pp. 166–175. (In Russian)

37. Nimis, P. Clinopyroxene geobarometry of magmatic rocks. Part 2. Structural geobarometers for basic to acid, tholeiitic and mildly alkaline magmatic systems. *Contrib. Mineral. Petrol.* **1999**, *135*, 62–74. [CrossRef]

38. Putirka, K.D. Thermometers and Barometers for volcanic systems. *Rev. Mineral. Geochem.* **2008**, *69*, 61–120. [CrossRef]

39. Himmelberg, G.R.; Loney, R.A. *Characteristics and Petrogenesis of Alaskan-Type Ultramafic–Mafic Intrusions, Southeastern Alaska*; U.S. Geological Survey Professional Paper 1564; US Government Printing Office: Washington, DC, USA, 1995.

40. Green, D.H.; Schmidt, M.W.; Hibberson, W.O. Island-arc ankaramites: Primitive melts from fluxed refractory lherzolitic mantle. *J. Petrol.* **2004**, *45*, 391–403. [CrossRef]

41. Pushkarev, E.V. *Petrology of the Uktus Dunite-Clinopyroxenite-Gabbro Massif (the Middle Urals)*; Russian Academy of Sciences, Ural Branch, Institute of Geology and Geochemistry: Ekaterinburg, Russia, 2000; p. 296. (In Russian)

42. Khedr, M.; Arai, S. Petrology of a Neoproterozoic Alaskan-type complex from the Eastern Desert of Egypt: Implications for mantle heterogeneity. *Lithos* **2016**, *263*, 15–32. [CrossRef]

43. Deng, Y.; Yuan, F.; Zhou, T.; Xu, C.; Zhang, D.; Guo, X. Geochemical characteristics and tectonic setting of the Tuerkubantao mafic-ultramafic intrusion in West Junggar, Xinjiang, China. *Geosci. Front.* **2015**, *6*, 141–152. [CrossRef]

44. Kay, S.M.; Kay, R.W. Aleutian tholeiitic and calc-alkaline magma series I: The mafic phenocrysts. *Contrib. Mineral. Petrol.* **1985**, *90*, 276–290. [CrossRef]

45. Singer, B.S.; Myers, J.D.; Frost, C.D. Mid-Pleistocene lavas from the Seguam volcanic center, central Aleutian arc: Closed system fractional crystallization of a basalt to rhyodacite eruptive suite. *Contrib. Mineral. Petrol.* **1992**, *110*, 87–112. [CrossRef]

46. Le Bas, M.J. The role of aluminum in igneous clinopyroxenes with relation to their parentage. *Am. J. Sci.* **1962**, *260*, 267–288. [CrossRef]

47. Loucks, R.R. Discrimination of ophiolitic from nonophiolitic ultramafic-mafic allochthons in erogenic belts by the Al/Ti ratio in clinopyroxene. *Geol. J.* **1990**, *18*, 346–349. [CrossRef]

48. Yogodzinsky, G.M.; Kelemen, P.B. Slab melting in the Aleutians: Implications of an ion probe study of clinopyroxene in primitive adakite and basalt. *Earth. Planet. Sci. Lett.* **1998**, *158*, 53–65. [CrossRef]

49. Izokh, A.E.; Vishnevskii, A.V.; Polyakov, G.V.; Kalugin, V.M.; Oyunchimeg, T.; Shelepaev, R.A.; Egorova, V.V. The Ureg Nuur Pt-bearing volcanoplutonic picrite–basalt association in the Mongolian Altay as evidence for a Cambrian–Ordovician Large Igneous Province. *Russ. Geol. Geophys.* **2010**, *51*, 521–533, 665–681. [CrossRef]

50. Oyunchimeg, T.; Izokh, A.E.; Vishnevsky, A.V.; Kalugin, V.M. Isoferroplatinum mineral assemblage from the Burgastain Gol placer (Western Mongolia). *Russ. Geol. Geophys.* **2009**, *50*, 863–872, 1119–1130. [CrossRef]